Lithos 288–289 (2017) 191–213

Contents lists available at ScienceDirect

Lithos

journal homepage: www.elsevier.com/locate/lithos

Petrogenesis of the postcollisional Middle Devonian monzonitic to granitic magmatism of the Sierra de San Luis, Argentina

Mónica G. López de Luchi [a,*], Siegfried Siegesmund [b], Klaus Wemmer [b], Nicole Nolte [b]

[a] Instituto de Geocronología y Geología Isotópica (INGEIS), CONICET-UBA, Facultad de Ciencias Exactas y Naturales, Intendente Güiraldes 2160, Ciudad Universitaria, C1428EGA, Argentina
[b] Geoscience Centre of the Georg-August University, Göttingen (GZG), Goldschmidtstr. 3, 37077 Göttingen, Germany

ARTICLE INFO

Article history:
Received 11 December 2016
Accepted 27 May 2017
Available online 7 June 2017

Keywords:
Petrogenesis monzonite and granite suites
Postcollisional magmatism
Middle Devonian
Sierra de San Luis
Sierras Pampeanas
Argentina

ABSTRACT

Middle Devonian granitoids intruded the Eastern Sierras Pampeanas basement ca. 600 km east of the inferred proto-Pacific margin of Gondwana along which a ca. 390 Ma collisional event developed. In the Sierra de San Luis, voluminous Middle Devonian (393–382 Ma) batholiths are composed of I- to A-type hybrid Monzonite and Granite suites. Shoshonite and subordinated high-K series, stocks, synplutonic dikes and enclaves make up the Monzonite Suite; rocks are metaluminous alkali–calcic magnesian porphyritic or equigranular monzonite, quartz monzonite, monzodiorite and scarce monzogabbro. High-K and subordinated shoshonite series metaluminous to mildly peraluminous magnesian alkali–calcic to calc–alkalic porphyritic or equigranular quartz monzonite, granodiorite, monzogranite and equigranular leucomonzogranites make up the Granite Suite plutons and batholiths. Only a small group of highly evolved granites are ferroan. SiO_2 (46–62%), Cr, Ni, V, Sc, LILE, LREE, Th, Zr and variable, Sr/Y, $(La/Yb)_N$ and $(Tb/Yb)_N$, smooth Eu/Eu*, moderate Na_2O (ca 3.5), and troughs at Nb and Ta for Monzonite Suite rocks suggest an subduction-related enriched lithospheric mantle source. Sm–Nd data (T_{DM} 0.98–1.08 Ga, $\varepsilon Nd_{(380\ Ma)}$ 0.66–1.47) and $^{87}Sr/^{86}Sr_i$ (0.703520–0.704203) are compatible with an enriched mantle source. The metaluminous porphyritic quartz monzonite–monzogranite and the mildly peraluminous equigranular biotite monzogranites of the Granite Suite are characterized by relatively moderate Al_2O_3, CaO, and $^{87}Sr/^{86}Sr_i$, high LILE, Cr, variable Sr/Y, $(La/Yb)_N$ and Eu/Eu* and low Rb/Sr (<1.2) suggest a mafic source. The porphyritic monzogranite (T_{DM} 1.20–1.28 Ga, $\varepsilon Nd_{(380Ma)}$ −3.02 to −3.3, $^{87}Sr/^{86}Sr_i$ 0.706578–0.707027) and the biotite monzogranites (T_{DM} 1.31 Ga, $\varepsilon Nd_{(380Ma)}$ −3.3, $^{87}Sr/^{86}Sr_i$ 0.707782) would share a common source. The equigranular alkali–calcic leucomonzogranites are characterized by Rb/Sr >1.5, ASI 1.05–1.18, and Ga/Al 2.6–3.9, $\varepsilon Nd_{(380\ Ma)}$ −3.74 to −3.95 and $(^{87}Sr/^{86}Sr)_i$ 0.710743–0.712955 which would point to metasedimentary or felsic igneous crustal sources. Nevertheless their T_{DM} 1.36–1.38 Ga is considerably younger than the mean 1.8–1.6 Ga Eastern Sierras Pampeanas crustal residence age and less radiogenic. Middle Devonian magmatism would record an episode of crustal growth by enriched mantle derived magma input and variable degrees of partial melting of a lower crustal source at the waning stages of the Achalian orogeny.

1. Introduction

High-K calc–alkaline and shoshonitic granitoid magmatism are common features of several orogenic belts. They are characterized by different scales heterogeneities, ranging from mineral zoning, xenocryst, mafic clots, mafic enclaves, stocks, and synplutonic dikes. Some of these features are attributed to mantle input and magma mixing and mingling. The overall tectono-magmatic evolution of these granitoids is associated with an extensional regime which could be related to the transition from a magmatic-arc to a post-collisional setting (Altherr et al., 2000; Bonin, 2004; Ferré and Leake, 2001; Janoušek et al., 2000; Jiang et al., 2002; López-Moro and López-Plaza, 2004; Topuz et al., 2010, and references therein) or to the back-arc extension of a distant subduction zone (Bussy et al., 2000; Fu et al., 2012; Yao-Hui et al., 2006, and references therein).

The Proto-Andean Pacific margin of Gondwana in central Argentina constitutes a long-lived orogenic system which covers the time span from the Neoproterozoic to Devonian (Cawood, 2005; Ramos, 2008; Rapela et al., 2007; Siegesmund et al., 2009), particularly in the Eastern Sierras Pampeanas of Central Argentina. The Sierras – a series of N–S polyphase deformed basement units cropping out between 26° to 33° S that were uplifted along Miocene-to-Recent reverse faults (Ramos et al., 2002)– are located between the Archaean-to-Palaeoproterozoic Río de la Plata craton to the east (Booker et al., 2004; López de Luchi et al., 2005; Rapela et al., 2007) and the Grenvillian (ca. 1000–1200 Ma, Kay et al., 1996) Cuyania-Precordillera terrane to the west. The Eastern Sierras Pampeanas were structured by three main events from the Neoproterozoic-to-Early-Cambrian (560–530 Ma) Pampean, the late Cambrian–Ordovician (500–460 Ma) Famatinian, and the

* Corresponding author.
E-mail address: deluchi@ingeis.uba.ar (M.G. López de Luchi).

http://dx.doi.org/10.1016/j.lithos.2017.05.018
0024-4937/

Devonian (400–350 Ma) Achalian orogenic cycles (Aceñolaza et al., 1988, 1990; Drobe et al., 2009, 2011; López de Luchi et al., 2007, 2010; Pankhurst et al., 1998; Ramos et al., 1986; Rapela et al., 1998, 2001, 2007; Siegesmund et al., 2004, 2009; Sims et al., 1997, 1998; Steenken et al., 2004, 2006, 2008, 2011; Stuart-Smith et al., 1999). These orogenies are related to the accretion of different terranes integrated into the proto-Andean margin of Gondwana and are accompanied by an extensive Palaeozoic granitoid magmatism. The Achalian suite of Middle-Devonian-to-Lower Carboniferous batholiths (López de Luchi, 1996; López de Luchi et al., 2004, 2007; Pinotti et al., 2002; Siegesmund et al., 2004; Stuart-Smith et al., 1999) were previously considered as-post-orogenic regarding the Famatinian orogeny (Rapela et al., 1998). The 393–360 Ma Devonian magmatism is mainly developed in the Sierra de Córdoba and San Luis (Fig. 2), whereas Lower Carboniferous magmatism is more conspicuous towards the north in the Sierra de Velasco and Fiambalá (Fig. 1a, b).

In the Sierras de San Luis (Figs. 1b, 2), Middle Devonian batholiths (Devonian Monzonite-Granite suite, DMGS, López de Luchi et al., 2007) are characterized by the ubiquitous occurrence of mafic monzonitic and more rare diorite rocks as microgranular enclaves, stocks, or synplutonic dikes in more felsic hosts or lamprophyre dikes, which would suggest a direct chemical and thermal input from the mantle (López de Luchi, 1996; López de Luchi et al., 2007). This magmatism is syn-kinematic with a system of shear zones that were active at the waning stages of the Achalian orogeny (López de Luchi et al., 2007; Siegesmund et al., 2004). In addition to longstanding questions about the details of the tectonic scenario for this magmatism (Llambías et al., 1998; López de Luchi et al., 2007; Siegesmund et al., 2004; Sims et al., 1998) which developed at 600 km of the inferred continental and collisional margin (Willner et al., 2011), it is important to evaluate crustal melting and the relative contributions of mantle-derived and crustal-derived melts to the construction of these upper crustal plutons.

The aim of this study is to analyze the petrogenesis of the main Middle Devonian batholith of the Sierra de San Luis. We integrate available geological, geochemical, and isotopic information with new chemical and isotopic data. Geochemical criteria are used for distinguishing and characterizing the coeval magmatic suites, and a petrogenetic model is formulated to account for the observed geochemical variations. This model, based upon major elements, trace elements, and Sr–Nd isotopes, allows constraints to be placed on the possible sources and processes that were involved in the genesis of the voluminous Devonian magmatism.

2. Regional setting

The Sierra de San Luis (Fig. 1b) records an Ediacaran-to-Devonian metamorphic and magmatic evolution (Siegesmund et al., 2009; Steenken et al., 2006, 2008) and comprises three NNE–SSW striking basement domains of amphibolite-to-granulite-facies ortho- and paragneisses, schists, migmatites, and amphibolites: namely, from west to east, the Nogolí, Pringles, and Conlara Metamorphic Complexes (Sims et al., 1997), separated by low grade rocks of the San Luis Formation (Prozzi and Ramos, 1988) and first intruded by Famatinian (500–480) (ultra-)mafic-to-monzogranitic units(López de Luchi et al., 2007; Sims et al., 1997, 1998).

Middle Devonian, voluminous zoned granitoid batholiths associated with monzonitic units (Figs. 1, 2) are represented by the Las Chacras-Potrerillos (LCHPB), Renca (RB), and La Totora batholiths (LTB) (López de Luchi et al., 2004, 2007; Siegesmund et al., 2004), as well as the San José del Morro (SJMP) (Quenardelle, 1995) and El Hornito (EHP) plutons. Field observations and geochemical and structural data suggest that they are pulsed, composite discordant intrusions with clear-cut contacts against the host Conlara Metamorphic Complex (Table 1). Al-in hornblende thermobarometer (Anderson, 1996) indicated ≈720 ± 15 °C and 3.55–3.84 ± 0.28–0.36 Kb (13–13.8 ± 1.1 km) for the emplacement of the granitoids of LCHPB and 730 ± 7 °C and 3.37 ± 0.6 kb (12.4 ± 2.2 km) for the Renca Batholith (Iannizzotto and López de Luchi, 2012; López de Luchi et al., 2007). The youngest cooling age (Table 1) corresponds to the BRG of the LCHPB and the oldest to the porphyritic facies of the LTB, i.e. the La Porteña Granite. Muscovite cooling ages are older for a pegmatite of PG of the LCHPB and the younger for NYF (niobium-yttrium-fluorine) pegmatite of the GPG. Monzonitic rocks are compositionally more variable in the RB however, they constitute more extensive outcrops, i.e. GPG, in the LCHPB. These regional variations in modal composition and cooling ages might suggest that the batholiths formed from distinct magmatic pulses (Lopez de Luchi et al., 2001, 2007).

A well-developed magmatic foliation, sometimes accompanied by high temperature solid-state deformation microstructures suggest a continuum from magmatic to high-temperature solid-state deformation during crystallization and initial cooling. The different batholiths were interpreted to be positioned at the crossover of coeval NNW–SSE sinistral transtensional and NNE–SSW transpressional shear zones that led to a NNE–SSW directed extension, allowing the formation of magma conduits. Middle Devonian crystallization age of the batholiths slightly post-dated the proposed 390 ± 2 Ma age (Willner et al., 2011) for the collision of Chilenia along the Gondwana margin (Table 1) whereas cooling ages are mostly coeval with the Ar/Ar muscovite ages of 375 to 351 Ma that constrain the activity of the NNE–SSW Río Guzmán shear zone (Sims et al., 1998).Therefore, the Devonian batholiths were considered syn-late collisional with respect to the Chilenia collision and syn-kinematic in relation with later compressional event related to strike slip shear zones (López de Luchi et al., 2002, 2004, 2007; Siegesmund et al., 2004).

3. Main lithological features

The studied Devonian batholiths and plutons are lithologically zoned, and two major magmatic associations can be defined petrographically (Fig. 3): i) a Monzonite Suite (MS) represented by monzonitic, monzodioritic and monzogabbric enclaves, as well as synplutonic dikes and porphyritic monzodioritic-to-quartz monzonitic stocks and ii) a Granite Suite (GS) that constitutes the more extensive outcrops (Fig. 2) and encompasses foliated to weakly foliated or locally unfoliated medium to coarse-grained equigranular or porphyritic quartzmonzonite, monzo and syenogranites (Table 1, Fig. 2). Batholiths are strongly zoned, whereas plutons are dominated by porphyritic monzogranites (Fig. 2, Table 1). Patterns of zonation are simpler in the RB and LTB, an external foliated biotite–amphibole granodiorite-monzogranite-quartz-monzonite coarse-grained porphyritic zone and a central equigranular to slightly inequigranular biotite monzogranite with a core of biotite–muscovite syenogranite. The LCHPB exhibits a complex pattern of multiple zoned intrusions, each of them with an external porphyritic facies and a central equigranular one (Brogioni, 1993; López de Luchi et al., 2001, 2007). In general, contacts among the different units of the batholiths are clearly delineated. GS contains xenolithic enclaves locally derived from the metamorphic country rocks. Since they concentrate in the marginal parts of the pluton or near metamorphic septa (López de Luchi et al., 2002, 2004).

Circular to elliptical, and centimeter- to meter-sized mafic microgranular enclaves (MME) are ubiquitous in isolation or as swarms in the stocks of the MS and in the porphyritic facies of the GS. MME were separated in five types (Table 2) based on the petrographic features, modes and chemistry (see Geochemistry chapter). Types 1 and 4 are porphyritic whereas Types 2, 3 and 5 are equigranular. Porphyritic vaugnerite Type 1 MME as well as durbachite Type 4 MME are larger and distinctively more abundant in the porphyritic granite, the less evolved unit of the GS. Type 1 MME are elongated, usually with their major axis parallel to the magmatic foliation (López de Luchi et al., 2004) which suggest that they shared a common magmatic deformation stage with their hosts and intruded in an still unsolidified granite;

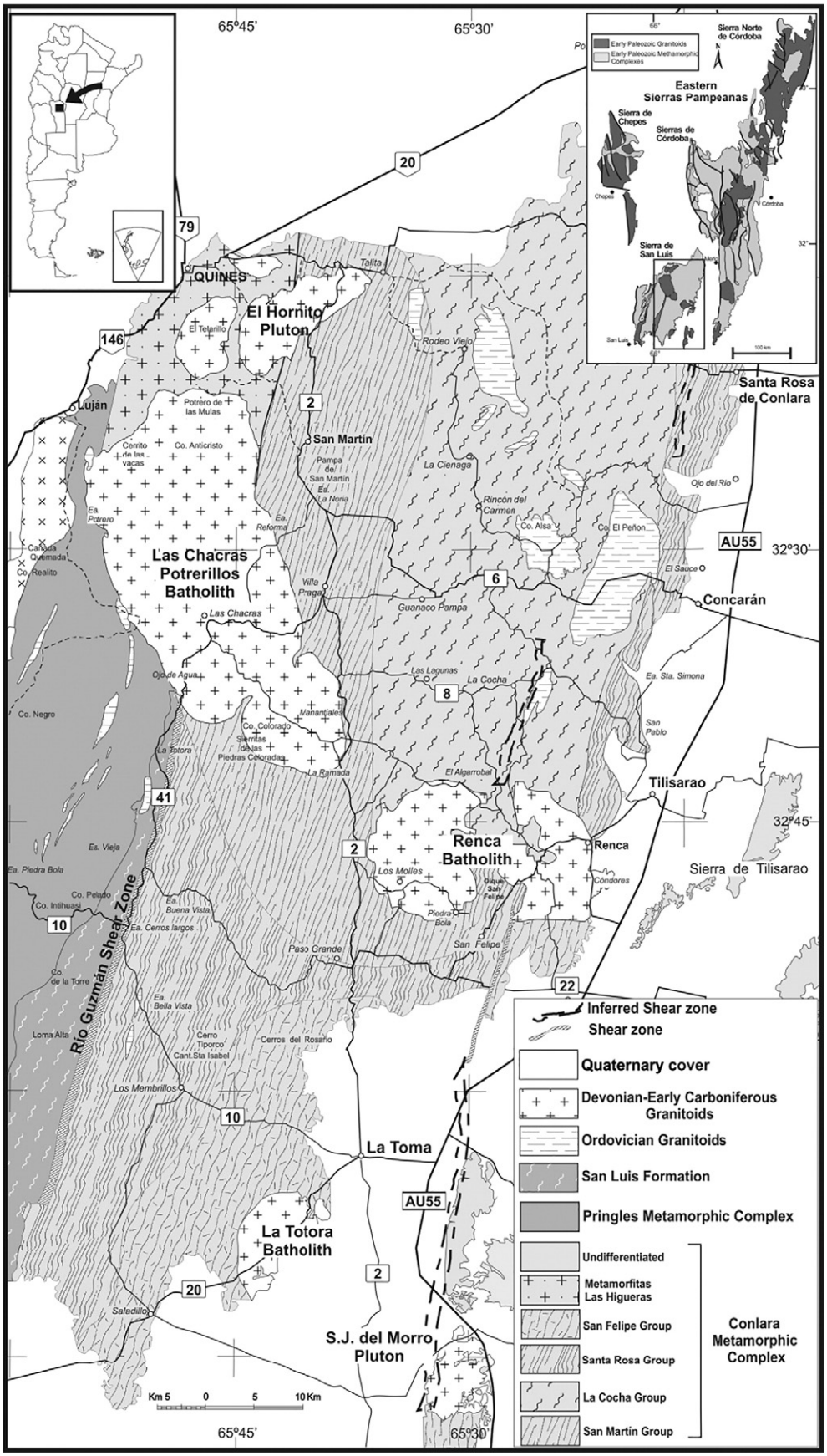

Fig. 1. Simplified geological maps: (a) Eastern Sierras Pampeanas; (b) Conlara Metamorphic Complex and the Ordovician and Devonian plutons and batholiths.

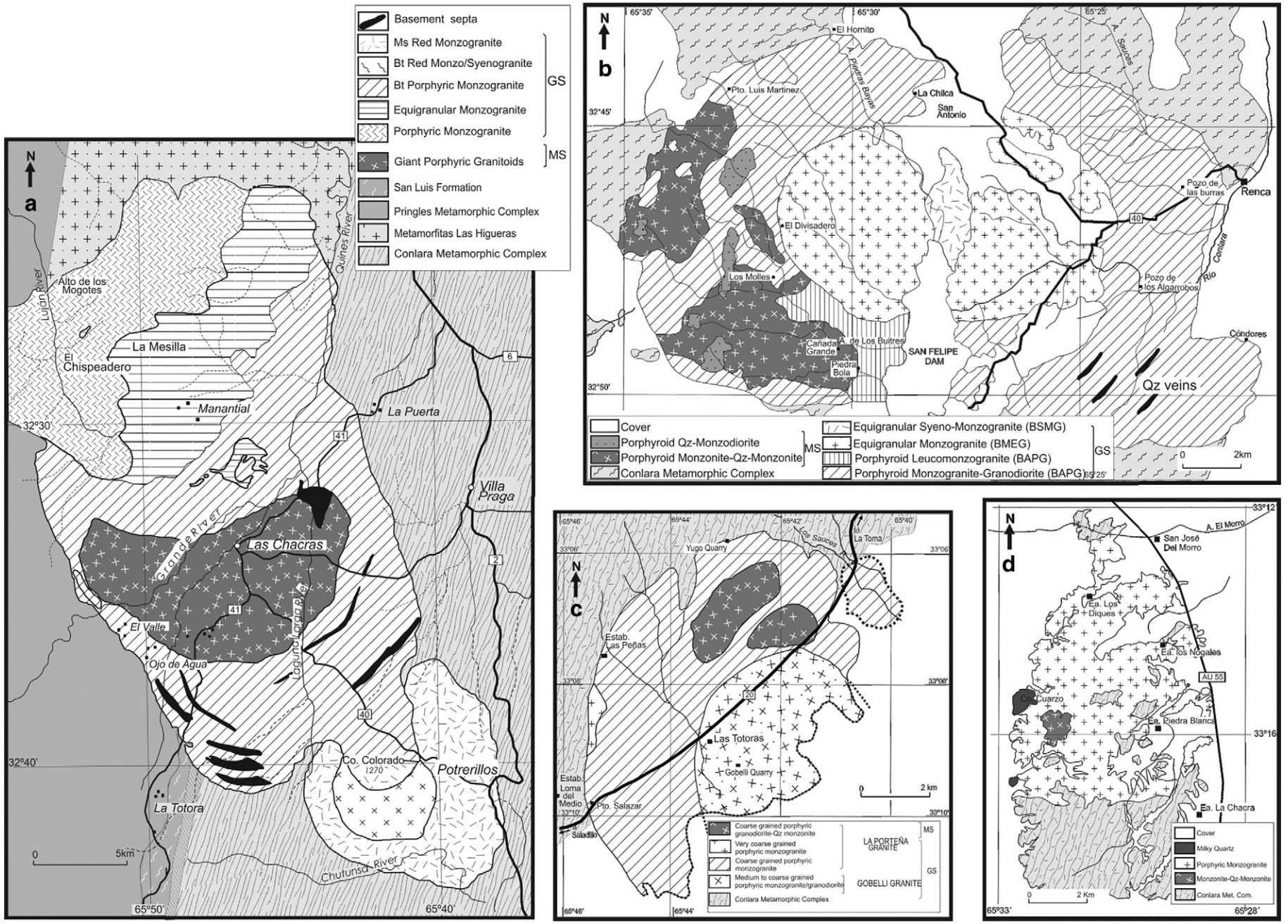

Fig. 2. Simplified geological maps of the four plutons studied: a) Las Chacras-Potrerillos Batholith modified after Siegesmund et al. (2004); b) Renca batholith modified after López de Luchi (1996), López de Luchi et al. (2004); c) La Totora Batholith modified after López de Luchi et al. (2004); d) San José del Morro pluton, modified after Quenardelle (1995).

Table 1
Summary of the facies, main lithologies, crystallization and cooling ages of the studied batholiths and plutons. EHP: El Hornito Pluton, LCHPB: Las Chacras-Potrerillos Batholith, RB: Renca Batholith, LTB: La Totora Batholith, SJMP: San José del Morro Pluton.

Unit		Facies	Main Lithologies	U–Pb (Ma)	K–Ar (Ma)			Rb–Sr (Ma)	Ref.
					Am	Ms	Bt		
EHP	Granite Suite		Biotite porphyritic monzogranite				343 ± 3		1,2
			Biotite equigranular monzogranite						
LCHPB	Granite Suite	MRG	Muscovite equigranular monzogranite						3,4,5
		BRG	Biotite–muscovite equigranular monzogranite ± syenogranite				335 ± 17		
		BPG	Biotite–amphibole porphyritic monzogranite	382 ± 5			362 ± 8		
				Zr			352 ± 7		
		EG	Biotite miarolitic equigranular monzogranite				349 ± 7	417 ± 16*	
			Biotite ± muscovite equigranular monzogranite						
		PG	Biotite porphyritic monzogranite/granodiorite						
		Peg in PG				381 ± 9			
	Monzonite Suite	GPG	Porphyritic Bt–Am Q monzonite	379 ± 69	345 ± 12		350 ± 7		1,5
			Porphyritic Bt–Am Q monzodiorite	Tit	368 ± 34				
		Peg in GPG				348 ± 8	357 ± 7		
RB	Granite Suite	BAPG	Biotite–amphibole porphyritic monzogranite/granodiorite	393 ± 5			346 ± 8		6,7,8
				Zr					
		BMEG	Biotite–muscovite equigranular monzogranite-leucomonzogranite			367 ± 9			
		BSMG	Biotite syeno–monzogranite						
	Monzonite Suite	ABPM	Biotite–amphibole porphyritic quartz monzonite						
			Amphibole–biotite porphyritic monzonite						
SJMP	Granite Suite	BPMG	Biotite porphyric monzogranite–syenogranite				365 ± 15	382 ± 4	9
								367 ± 15	
	Monzonite Suite	BAPQM	Biotite–amphibole porphyritic quartz monzonite		360 ± 20				
LTB	Granite Suite	Gobelli	Biotite porphyritic monzogranite/quartzmonzonite				358 ± 8		10,11
		La Porteña	Biotite–amphibole porphyritic monzogranite				371 ± 8		
	Monzonite Suite	PQMZ	Biotite–amphibole porphyritic quartz monzonite						

1 Steenken et al., 2002; 2 Ortiz Suárez et al., 2009; 3 Brogioni, 1991, 1993;4 Lopez de Luchi et al., 2001; 5 Siegesmund et al., 2004; 6 López de Luchi, 1986, 1987, 1996; 7 Lopez de Luchi et al., 2001; López de Luchi et al., 2002; 8 Sims et al., 1997, 1998;9 Quenardelle, 1995; 10 López de Luchi et al., 2002; 11 Steenken et al., 2002; *recalculated after Brogioni (1991) data.

disaggregation of syn-plutonic dykes along the strike led to the generation of Type 4 MME. The contact with the host monzogranite or quartz monzonite of the GS is variable from diffuse to rather sharp, or lobate with interfingering with the MS stocks. Vaugneritic breccia along the contact between monzonite stocks suggest that the porphyritic monzogranites of the RB are slightly younger than the monzonite stocks, whereas, in the LCHPB enclaves of BPG inside GPG indicate that this monzonite stock is younger. Type 3 equigranular durbachite enclaves which are found only in the monzonitic stocks as well as Types 2 and 5 MME are aphyric, normally more spheric in shape, and locally with quenched margins.

Porphyritic Types 1 and 4 MME and stocks are amphibole biotite monzonite, monzodiorite, i.e. vaugnerite and durbachite and are characterized by variably perthitic and poikilitic microcline megacryst — mostly of the same the size than those of the host porphyritic granitoid. Some megacrysts cut across the contact between the enclave and granite host, whereas others are completely included, especially in the porphyritic monzonite stocks or along the border of the synplutonic dikes.

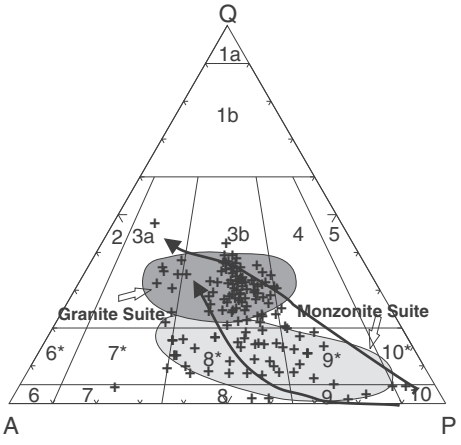

Fig. 3. QAP modal plot for representative samples of the Devonian granitoids. Modal composition mostly plots between the calc–alkaline medium K granodioritic (a) and the high K monzonitic (b) magmatic differentiation trends. Rocks with modal Q below 20% correspond to stocks, MME and syn-plutonic dikes, where those in the fields above 20% belong to the Granite Suite that is represented by the most voluminous facies of the batholiths and plutons.

MME typically show igneous fine grained textures with acicular apatite, quartz ocelli and felsic segregation surrounded by amphibole–biotite. The most common dm-to-m Types 1, 3, and 4 enclaves are monzonite, and silica-poor monzonite/monzodiorite (Table 2) and display fine-grained doleritic textures or an interlocking of anhedral poikilitic K-feldspar and/or quartz in their groundmass. Felsic ocellar structures as well as the K megacryst were related to thermal and compositional interactions of (hydrous) mafic magma batches with co-existing granitic magmas (López de Luchi, 1996).

4. Geochemistry

4.1. Chemical classification

Rocks were separated into two suites: Monzonite Suite (MS) with SiO_2 < 65% and Granite Suite (GS) with SiO_2 ≥ 65% (Figs. 3, 4a, Table 1). The two suites (Fig. 4a.1–3) define a smooth scattered negative slope for total alkalies (7–9%) from 55% SiO_2 to 76% SiO_2.

GS rocks are granodiorite, (monzo and minor syeno) granite and quartz monzonite and plot in the field of the transalkaline series when amphibole bearing or in the subalkaline series when biotite or biotite–muscovite bearing, i.e. the Red Granite and some samples of the Rodeo de Los Molles area of the Equigranular Granite of the LCHPB, some samples of the porphyritic monzogranite-granodiorite and the biotite–muscovite monzogranite of the RB, the Gobelli granite of LTB, a group of monzogranites of the SJMP and the only two samples of El Hornito pluton (Figs. 2, 4 a1–3). In the K_2O versus SiO_2 plot (Fig. 4b.1–3) porphyritic rocks of the GS straddle the fields of the high-K calc–alkaline and shoshonite series of Rickwood (1989). GS rocks are metaluminous to mildly peraluminous alkali–calcic and

Table 2
Main lithologies, chemical classification and host of the different mafic microgranular enclave (MME) types.

MME	Main lithologies	Chemical	LCHPB			RB	SJM		LT
		Classification	BPG	PG	GPG	BAPG	ABPM	MZ	LPG
Type 1	Low MgO amphibole biotite porphyrtic monzonite	Vaugnerite	X	X	X	X		X	
	Low MgO amphibole biotite monzonite-monzodiorite			X					
Type 2	Equigranular biotite ± amphibole monzonite–monzodiorite	Appinite				X			
Type 3	High MgO equigranular amphibole biotite monzonite	Durbachite					X		
Type 4	High MgO porphyritic amphibole biotite monzonite + monzodiorite	Durbachite				X	X		X
Type 5	Equigranular amphibole monzodiorite monzogabbro	Vaugnerite					X	X	

magnesian (Fig. 4c,d,e.1–3). Only the high-K series biotite–amphibole porphyritic granite from the RB are in the calc–alkaline field. Some samples with SiO_2 > 70% are ferroan, i.e. the Red Granite, and some Equigranular Granite from the LCHPB (Fig. 4c.1). Mineralogy supports the metaluminous-to-weakly-peraluminous character of these rocks because scarce primary muscovite only appears in the more evolved Red Granite rocks of the LCHPB and in the biotite muscovite equigranular Granite of the RB. Samples with ASI ˂1.2, correspond to the area near the REE mineralization of Rodeo de Los Molles in the NE sector of the LCHPB (Lira and Ripley, 1992) and probably exhibit a higher degree of alteration.

The Monzonite Suite rocks (46–65% SiO_2) are mostly monzonite enclaves, synplutonic dikes and stocks. Type 5 MME (Table 2) with SiO_2 from 45 to 50% are monzodioritic/gabbro whereas higher total alkalies Type 1 MME (50–55% SiO_2) of the Porphyritic Granite of the LCHPB and some enclaves of the RB plot along the limit between monzonite and foid-monzodiorite or monzosyenite (Fig. 4a, 1–2). MS belong to a transalkaline series, show scatter in both K_2O and FeOt / (FeOt + MgO and are metaluminous alkali to alkali–calcic and magnesian (Fig. 4a, b, c, d, e.1–3).

Most of the MS rocks plot in the field of shoshonitic series (Fig. 4b.1–3); one biotite monzonite enclave of the biotite amphibole porphyritic granodiorite-monzogranite as well as two samples of the monzonitic stocks of the Renca Batholith are located in the high-K series field.

In a K_2O versus MgO plot (Fig. 5a-b) (Ferré and Leake, 2001) these shoshonitic MS rocks can be further discriminated (Table 2). Type 1 MME are characterized by MgO between 2 and 4% and K_2O from 4-to 7% (they show a restricted ASI between 0.9 and 1) and correspond to amphibole–biotite porphyritic monzonite to quartz monzonite. Stocks are similar in MgO but with lower K_2O. Type 2 MME that are biotitic show MgO around 3% and K_2O from 2.5-to 4.5%. The aphyric monzonites Type 3 MME that are recognized only in the stocks and the porphyritic monzonite-monzodiorite Type 4 MME and synplutonic dikes exhibit the highest K_2O content and MgO between 5 and 7%. Type 5, the more mafic enclaves with SiO_2 from 45 to 50% that appear only in the monzonitic stock of the RB and in the SJMP are low K_2O and MgO rich rocks that plot as monzodiorite/gabbro. Chemical characteristics of the MS rocks are akin to the vaugnerites (stocks, Type 1 MME and monzogabbros/monzodiorites Type 5 MME) and durbachites (Types 3 and 4 MME) whereas Type 2 MME due to their low K_2O, plot towards the field of the appinites. The monzonite stocks are comparable to the vaugnerite series (Ferré and Leake, 2001 and references therein) of Corsica or the French Central Massif.

The overall geochemical features of MS rocks match the criteria established by Jiang et al. (2002, 2012) for shoshonitic type rocks since they have a) high K_2O and K_2O/Na_2O ratio between 1 and 2, as well as a high P_2O_5 and low SiO_2/P_2O_5 ratio, b) a high LREE and LREE/HREE ratio, (c) a high content of some LILE, such as Sr and Ba, as well as F (as indicated by the abundance of apatite) and (d) a relatively high to moderate $\varepsilon Nd_{(t)}$ and a relatively wider range in $(^{87}Sr/^{86}Sr)_i$. The relatively unevolved isotopic signature (see below) at least of the MS rocks of the LCHPB suggest source rocks not long separated from the mantle. This mantle imprint in granite batholith is typical of I-type magmatism (see Clemens et al., 2016 for discussion).

4.2. Whole rock major and trace element chemistry

The whole data collection, 46% to 76% SiO_2, displays a large range for major and trace elements (Figs. 6 and 7).The Type 1 MME (vaugnerites), monzonite stocks and the porphyritic granitoids of the GS generally plot along the same trends whereas there is significantly more scatter in the MME and syn-plutonic dikes trends as well as in the more evolved equigranular monzogranites or the Red granites of the LCHPB. Ba, Rb, Sr, Ga, Zr, Y, LREE, and REE_t are distinctly higher in average for the MS than for the GS (Fig. 7, Supplementary Table 1) except for Type 5 MME of the RB and San José del Morro pluton. Chondrite-normalized REE diagram and the OIB, lower and upper crustal normalized trace-element patterns of the stocks of the MS and the GS rocks (Fig. 8) are parallel similarly to those of the MME (Fig. 9). They share a comparably steep left–right slope, negative Nb anomalies and variable Th abundances (data only for RB) which generate either peaks or troughs on the normalized patterns. The monzonite stocks rocks plot systematically above the porphyritic granitoids being more pronounced the troughs at P and Ti for the latter (Fig. 8b, c, d.1–3). The equigranular biotite granites like those of RB or the Gobelli granite of the LTB (Fig. 8b, c, d.1–3) plot separately and with a general impoverishment in REE and more pronounced troughs at P and Ti.

GS rocks (SiO_2 > 65%) define negative continuous trends for most elements from the porphyritic quartz-monzonites to monzogranites (Figs. 6, 7a–e.1–3) except for a positive slope for Na_2O and variable K_2O. Biotite–amphibole-porphyritic granitoids like BAPG of the Renca Batholith exhibit higher Ba and Sr contents than the biotite one. Rb mainly correlate positively with SiO_2 for the biotite porphyritic Granite of the LCHPB whereas it exhibits a smooth negative slope in the RB, LTB and the plutons. PG of the LCHPB show positive slope for Sr, negative slope for Zr and scatter in Ba and Rb. Equigranular monzogranites and leuco-monzogranites, show scattered patterns with SiO_2 increase being potassium higher than for the porphyritic granites at a certain sodium content. Patterns for Y and Nb (Fig. 7f, g.1–3) exhibit a marked increase in the highly differentiated granitoids of the LCHPB. Typical continental crust values for Nb/Ta ˂12 are shown by the granites of RB and the BPG of the LCHPB.

MS stocks and Type 1 MME of the RB and LCHPB show Fe_2O_{3t}, TiO_2 (not shown), MgO, CaO, and P_2O_5 displaying a straight, negative,

Fig. 4. Chemical classifications for the whole data set of the monzonite and granitoid suites. Data recalculated to 100% on a water-free basis: a) TAS diagram (Middlemost, 1994, 1997) for plutonic rocks. The curved dashed lines separate alkali and transalkaline from subalkaline rocks. Note that total alkalies are almost constant except for two enclaves of the RB; b) K_2O vs. SiO_2 plot of Rickwood (1989); c) and d) Chemical classification diagrams and representative fields of Frost et al. (2001). c) FeO tot (FeOtot + MgO) vs. SiO_2(wt%). Samples with SiO_2 above 70% are located in the ferroan field only for the RG of the LCHPB; d) Modified alkali–lime index vs. SiO_2(wt%) showing the suites that were defined by Peacock (1931). Samples are located in the area of the alkalic and alkalic–calcic suites. The calc–alkalic suite corresponds only to a group of BAPG of the RB; e) Alumina saturation index (ASI) (Shand, 1943) plot. For equivalent ASI values, samples of RB are more variable in the Al_2O_3 / Na_2O + K_2O. Except for two samples of the EG of the LCHPB, the peraluminous samples exhibit ASI values below 1.15.

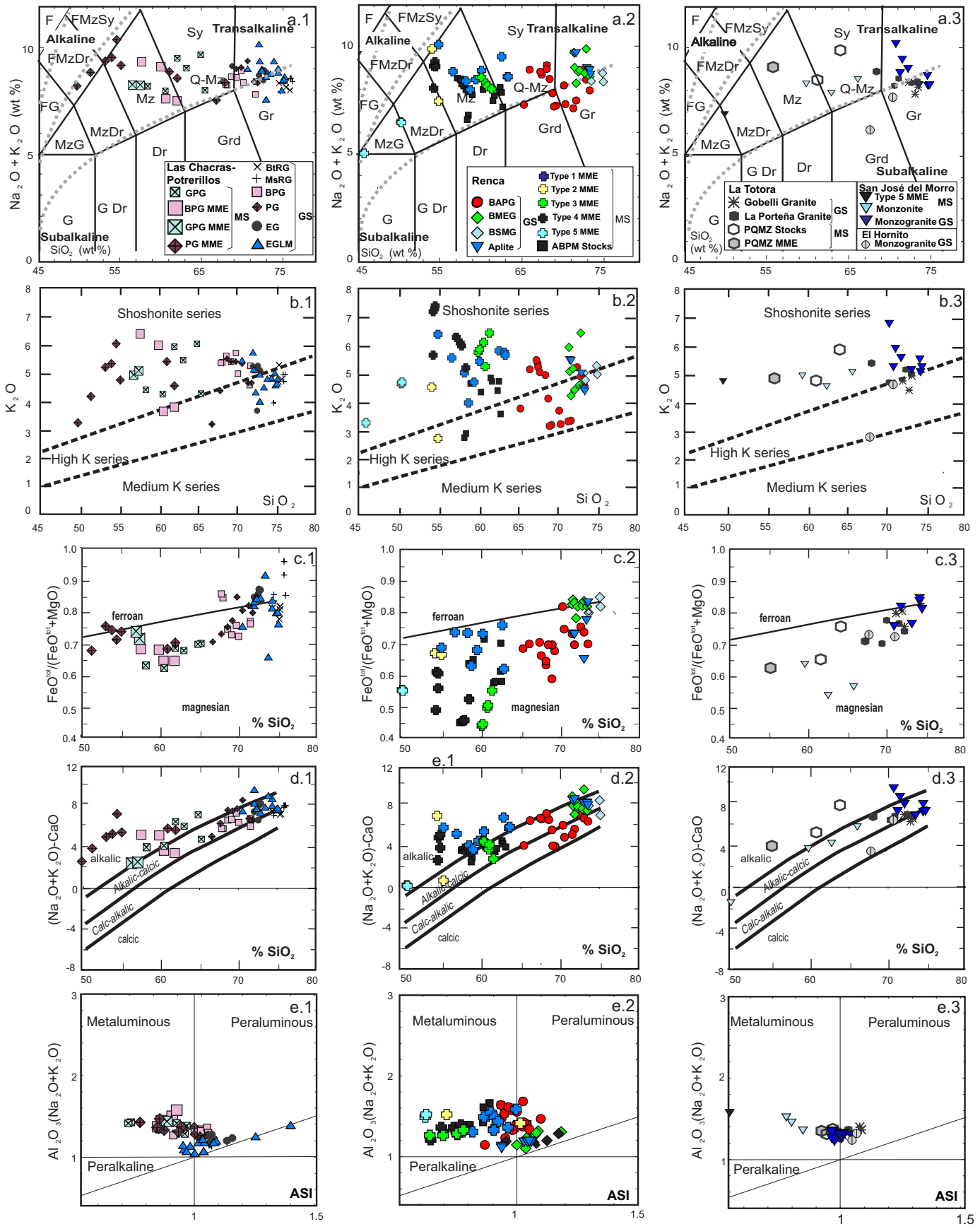
a.1
a.2
a.3
F
FMzSy
Alkaline
Sy
Transalkaline
FMzDr
Q-Mz
Mz
FG
Gr
MzDr
MzG
Grd
Dr
G Dr
G
Subalkaline
Na2O + K2O (wt %)
SiO2 (wt %)
Las Chacras-Potrerillos
GPG
BPG MME
GPG MME
PG MME
BtRG
MsRG
BPG
PG
EG
EGLM
MS
GS
Renca
BAPG
BMEG
BSMG
Aplite
Type 1 MME
Type 2 MME
Type 3 MME
Type 4 MME
Type 5 MME
ABPM Stocks
La Totora
Gobelli Granite
La Porteña Granite
PQMZ Stocks
PQMZ MME
San José del Morro
Type 5 MME
Monzonite
Monzogranite
El Hornito
Monzogranite
b.1
b.2
b.3
Shoshonite series
High K series
Medium K series
K2O
Si O2
c.1
c.2
c.3
ferroan
magnesian
FeOt/(FeOt+MgO)
% SiO2
d.1
d.2
d.3
alkalic
Alkalic-calcic
Calc-alkalic
calcic
(Na2O+K2O)-CaO
e.1
e.2
e.3
Metaluminous
Peraluminous
Peralkaline
ASI
Al2O3/(Na2O+K2O)

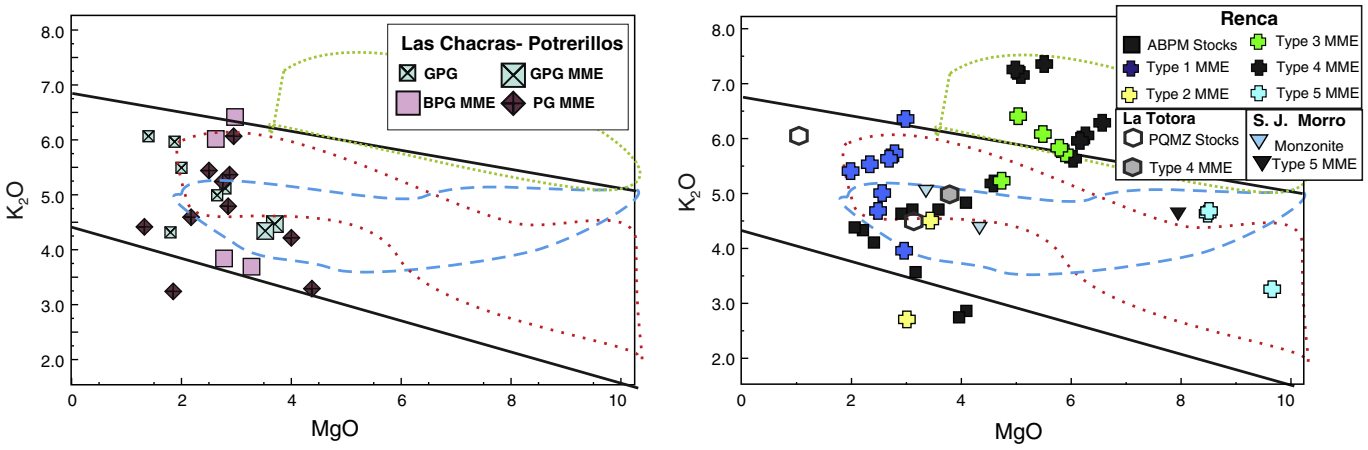

Fig. 5. K_2O vs. MgO wt% plot of Monzonite Suite rocks (SiO_2 < 65 wt%). Fields for vaugnerites from both Corsica (red dotted line), the French Central Massif (blue dashed line), and for durbachites (green dotted line) were taken from Ferré and Leake (2001). Rocks in the low-K field correspond to appinite of Scotland or low-K diorites of Corsica (Ferré and Leake, 2001).

continuous correlation with SiO_2 (Fig. 6a–f.1–2). In Type 1 MME Na_2O is almost constant whereas K_2O shows a highly disperse pattern (Fig. 6c, d.1–2) which reflects the variable modal content of K-feldspar megacrysts. Continuous trends show the variation in the modal amount of the main rock-forming minerals: K-feldspar, Mg-rich amphibole and biotite, plagioclase, titanite, magnetite, and apatite. The rest of the MME types do not define trends due to more limited range of SiO_2. Type 5 MME show the lowest Na_2O and Al_2O_3 and the highest CaO, Fe_2O_3 and MgO.

Type 1 MME and stocks of the RB and some Type 1 MME of BPG of the LCHPB show Sr between 300 and 700 ppm (Table 3). Type 1 MME of GPG and most of the PG are richer in Sr. Type 1 MME and stocks of the RB and the porphyritic granites of the GS delineate continuous negative slopes against SiO_2. Content of Sr are variable for the rest of the MME being Type 5 MME of the RB the poorer (Fig. 7a.2, Table 4). Ba shows a similar behavior (Fig. 7b.1–3). Rb and Zr are scattered for all the MS. The Rb content of the less evolved rocks of the MS is comparable to that of the Granite Suite. REE_t decrease as SiO_2 increases being Type 1 MME and stocks the richest in average (Table 3, Fig. 7c, d, e, f.1–3). Biotite equigranular monzogranites and the biotite–muscovite syenomonzogranite of the RB are poorer in REE than the porphyritic facies of GS and the MS rocks. Y and Nb (Fig. 7f, g.1–3) exhibit a slightly scattered negative slope. Nb/Ta is around chondrite values only for Type 5 MME, i.e. 18–20 whereas Nb/Ta is crustal for the rest albeit slightly higher than for the GS.

Eu/Eu_N^* decreases versus SiO_2 from 0.8 to 0.4 (Fig. 7h.1–3) for the whole data collection which indicates the strong control of plagioclase in the fractionation trends, from the stocks and Type 1 vaugnerites of the MS to the GS, which fits the negative slopes for Ba and Sr. Type 5 MME show Eu/Eu_N^* <0.65. La/Yb_N varies from 10 to 35 for most of the Monzonite and Granite suites. GPG of the LCHPB, Types 2 and 3 MME of the RB, and two monzogranites of La Porteña facies of the LTB show the higher La/Yb_N between 30 and 35 (Fig. 7i.1–3). Rb/Sr is lower than 1 except for the BMEG and BSMG of the RB (1.5–2.8) and the RG of the LCHPB (2–30).

The behavior of most trace elements, including REE, can be described as compatible, except Rb, Y, and Nb for the RG of the LCHPB (Table 2 and Fig. 7c, g, h.1–3). The observed trace element and REE characteristics are common to other high-K granitic suites and associated vaugnerites (Debon and Lemmet, 1999; Ferré and Leake, 2001).

Chondrite-normalized REE plots (Fig. 8a.1–3) for GS and the MS stocks show similar slopes and concave upward shapes that are more pronounced in some of the porphyritic granites of the GS. The La/Yb_N ratio is, on average, higher for the monzonite stocks of the RB coupled with a less pronounced Eu/Eu*. Since La/Yb_N and Eu/Eu* decreases with SiO_2 increase from vaugnerite stocks to the porphyritic monzogranites and quartz-monzonite of the Renca and Las Chacras Potrerillos batholith (Fig. 7i.1–2), fractionation of accessory REE bearing minerals would be associated with plagioclase fractionation. Chondrite normalized REE plots of the different MME types (Fig. 9a.1–3) indicate a decrease in $(La/Yb)_N$ coupled with increasing Eu/Eu*. Types 2 and 3 MME show high (30–35) $(La/Yb)_N$ with a steeper (3) $(Gd/Yb)_N$ for Type 3 which suggest the control by garnet on the source. Type 4 MME (Fig. 9a.2) are similar up to Eu but $(Gd/Yb)_N$ slope is smoothly negative and concave upwards. Type 5 MME (Fig. 9a.2) shows the lowest $(La/Yb)_N$ and a marked Eu/Eu*.

OIB normalized spider diagrams for the porphyritic granitoids (Fig. 8b.1–3) exhibit a negative slope from Rb to Y, LILE higher than OIB, trough at Nb-Ta for the RB and at Nb for the rest of the units and content close to OIB from La to Yb except for Ti. More negative Sr, P and Ti peaks are depicted by the highly differentiated granites of the RB, the Gobelli granite of the LTB as well as the monzogranites of the SJMP and EHP. MME (Fig. 9b.1–3) show enrichment in LILE together with troughs at Nb–Ta (only for the RB) or Nb for the rest of the units, and Ti are observed. From La to Y except for Ti, values are slightly higher than OIB for Types 1 to 4 MME and similar to OIB for Type 5 MME which also show lower La and Ce and a more pronounced Sr negative peak. Normalized P is lower for Type 2 MME (Fig. 9b.2).

Lower Crust normalized plots (Fig. 8c.1–3) show enrichments for the MS stocks whereas the porphyritic rocks of GS show values close to 1 for Sr, P, Zr and Ti. Equigranular granites show troughs for these elements but values close to 1 from Nb to Ce, Nd, Hf, Sm and Tb to Yb. MME plots (Fig. 9c.1–3) indicate that except for the enrichment in LILE the rest of the element contents are similar to the Lower Crust being Type 5 the one that exhibit normalized values closer to 1 (Fig. 9c.2). Upper crustal normalization plots are used in order to evaluate a likely sedimentary input as the signature of enrichment for the MS magma sources. Stocks of MS as well as porphyritic granitoids of GS exhibit values slightly above 1 from La to Tb whereas they are slightly below 1 for the equigranular granites of RB, LTB and SJMP. MME shows values above 1 except for Nb, Tb and P.

Apatite and zircon thermometry (Harrison and Watson, 1984; Jung and Pfander, 2007; Watson and Harrison, 1983) were applied to rocks with evidence of saturation in P_2O_5 and Zr. Zircon temperatures were calculated on the rocks of the GS that fulfilled the criteria of Zr saturation and the M value below 1.8 and where careful petrographic observations indicate that zircon is mostly an early phase that continues to crystallize until late stages. The GS yielded temperatures between 700 and 830 °C for the LCHPB, 740–810 °C for the RB, 780–840 °C for the LTB and 780–820 °C for the SJMP. The porphyritic quartz monzonite and

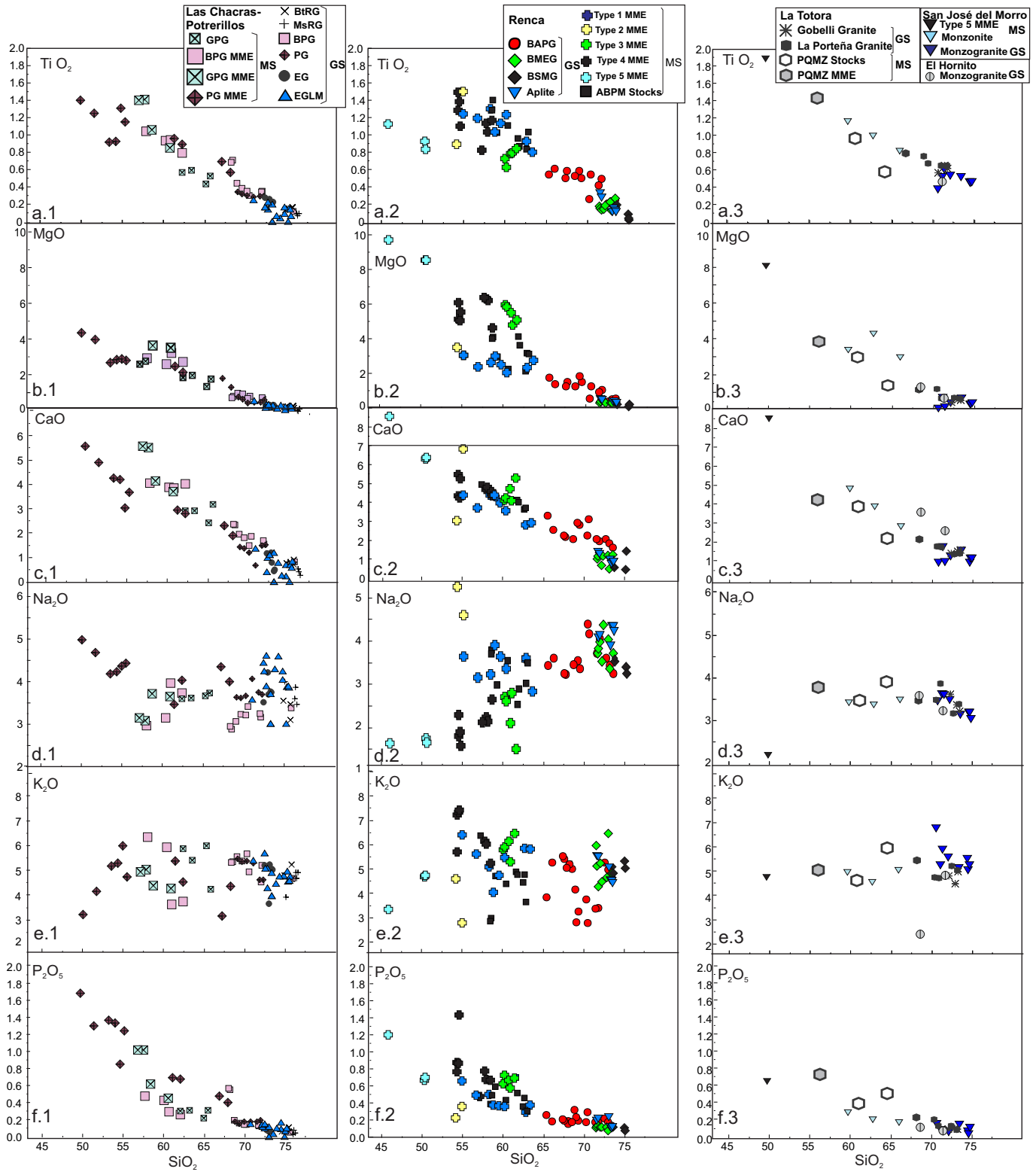

Fig. 6. Major element (wt%) variation diagrams vs. SiO_2 for the whole chemical data set. See text for comments. Symbols as in Fig. 4.

monzogranite exhibit the highest saturation temperature that agree with its less fractionated signature as evidenced by both the SiO_2 interval and the Zr content closer to the calculated Zr saturation. The apatite thermometer for the GS gives temperatures between 800 and 1020 °C whereas the monzonite stocks, MME and synplutonic dikes of the MS yielded temperatures between 900 and 1080 °C (Table 4).

5. Nd–Sr isotope systematics

Rb–Sr and Sm–Nd data are listed in Tables 3 and 4. $\varepsilon Nd_{(t)}$ versus $(87Sr/86Sr)i$ plot (Fig. 10a) were compared with compositional fields of the main Early Paleozoic components of the Sierra de San Luis as well as other Devonian plutons. Stocks of the RB and LCHPB exhibit

$(^{87}Sr/^{86}Sr)_i = 0.704203–0.704428$, $\varepsilon Nd(t) = -1.47–1.52$ and T_{DM} of 1.1 Ga The MMEs of the RB and the only available data for SJMP, i.e. a Type 4 MME have $(^{87}Sr/^{86}Sr)_i = 0.705,559–0.706829$ and $\varepsilon Nd(t) = -2.44$ to-4.84, and T_{DM} of 1.2 to 1.4 Ga. One equigranular monzonite MME of PG yielded $(^{87}Sr/^{86}Sr)_i = 0.703520$, $\varepsilon Nd(t) = -0.66$, and T_{DM} of 0.99 Ga being the more primitive rocks (Tables 3, 4).

GS rocks (Table 3, Fig. 10a, b, c) exhibit a restricted range of $\varepsilon Nd(t) = -3.02$ to -3.95, T_{DM} from 1.4 to 1.2 Ga and a wider range of $(^{87}Sr/^{86}Sr)i = 0.706474–0.711184$ for the RB, the SJMP and the BPG of the LCHPB. On the contrary PG and EG of the LCHPB are more primitive and are grouped with the MS stocks and MME of this batholith. Available data for the granitic rocks of the Devonian Alpa Corral Batholith (Pinotti et al., 2002) and for gabbroic to dioritic of the El Molle pluton (Sato et al., 2001) plot along the trend defined for most of the GS and the MS rock. Model ages calculated for the GS except for PG and EG of the LCHPB are consistent with the data presented by Sato et al. (2001) for El Molle pluton in the western part of the Sierra de San Luis. T_{DM} 1.75–1.54 Ga for the Sierra de San Luis Ordovician rocks indicates Paleo to Mesoproterozoic sources (López de Luchi et al., 2007) which is typical for the Ordovician Famatinian granites (Pankhurst et al., 1998, 2000; Rapela et al., 1998).

$\xi Nd_{(380\ Ma)}$ and $(^{87}Sr/^{86}Sr)_i$ values show a systematic variation with SiO_2 (Fig. 10b, c), indicating mixing for a part of the MS rocks and the GS. At a similar SiO_2 interval, Type 1 MME, MME of the PG and stocks of LCHPB and RB as well as PG and EG are significantly more primitive than the rest of the MME and granites of the GS. (Fig. 10b, c). These

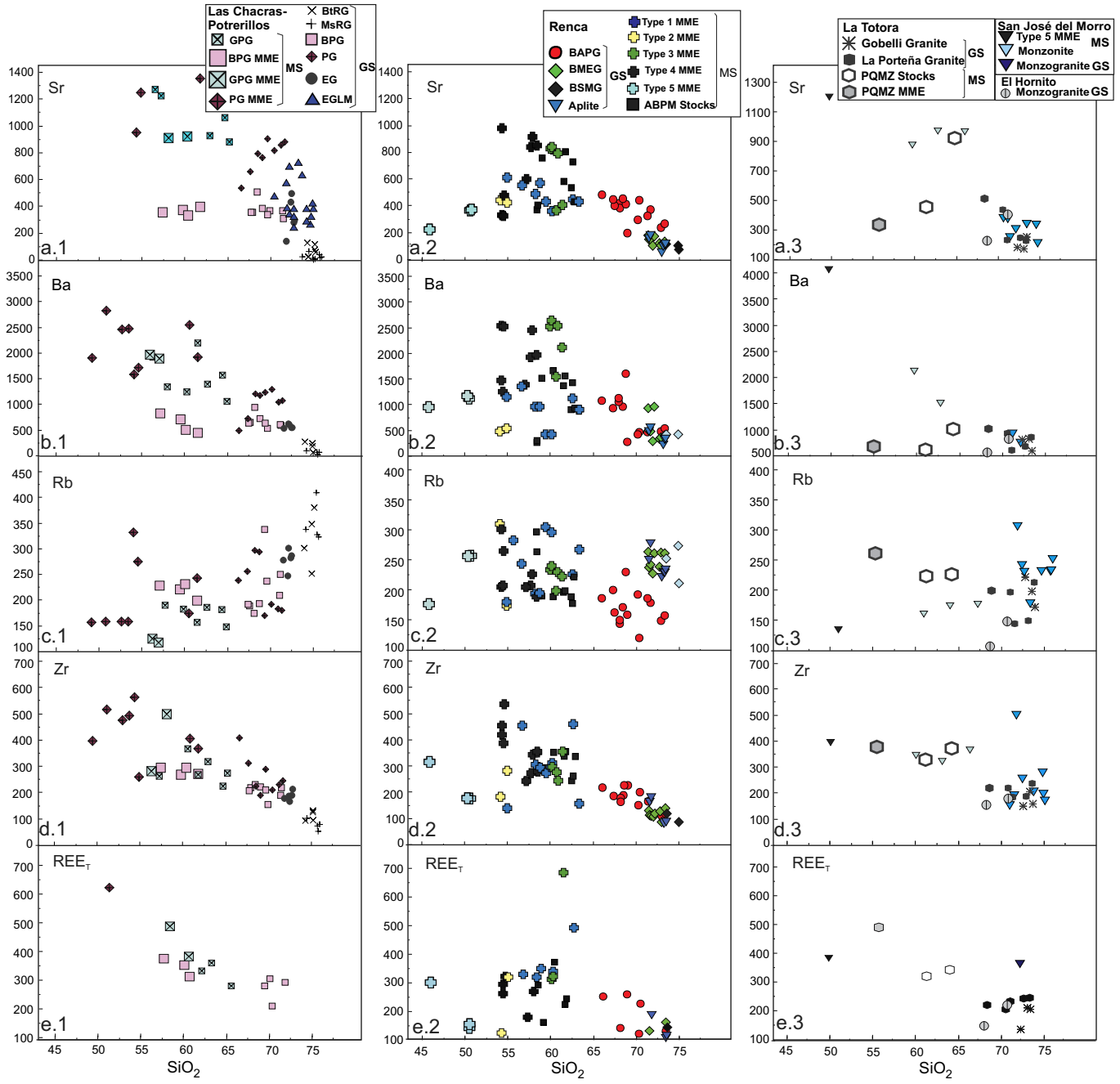

Fig. 7. a) Trace element (ppm) vs. SiO_2 for the whole chemical data set. See text for comments; b) Selected inter-element ratios plotted as variation diagrams vs. SiO_2 Symbols as in Fig. 4.

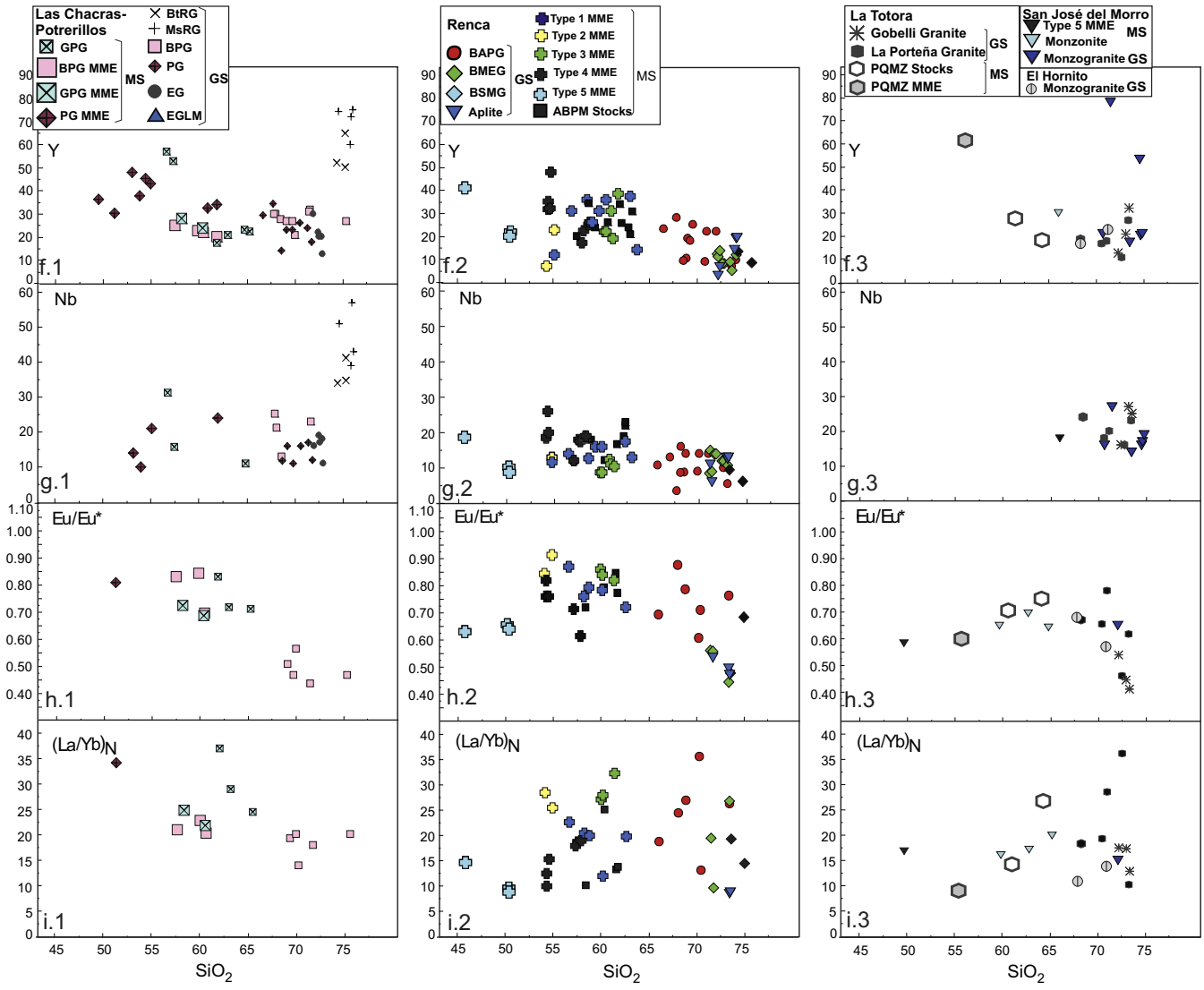

Fig. 7 (*continued*).

data suggest that at least different processes or mafic sources are involved. Mixing between a crustal derived magma and a primitive mafic magma could explain the continuous trends depicted between the more primitive magma represented by the MME of PG and source magmas for the GS.

6. Tectonic setting

Most of the rocks plot (Fig. 11a.1–3) in the fields of volcanic arc and syn-collisional granitoids (Pearce et al., 1984) which overlaps with the post-collisional field of Pearce (1996). In the Triangular plot Rb/30–Hf–Nb/4 (Harris et al., 1986) samples of the RB plot in the volcanic arc field whereas most of the granitoids of the LCHPB plot in the late to post-collisional field or in the syncollisional fields (Fig. 11b).

The rocks that plot in the WPG field (Fig. 11a.1–3) belong to the MS of the RB, LCHPB, TB and SJMP together with some GS units, i.e. samples of BPG and the BRG and the MRG. Only some MME, BRG and MRG show Ga/Al higher than 2.8 (Fig. 11c). Further chemical division of the A-type granites based on the discriminant ratios proposed by Eby (1992) indicates compositional similarity with A2-type based on the Y/Nb but except for the ferroan, RG of the LCHPB rocks are magnesian (Fig. 4b.1–3). The location in the A2 type suggest postcollisional granites or those that were emplaced at the end of a long period of apparently high heat flow and granite magmatism (Eby, 1992). In addition Y/Nb higher than 1 would indicate arc-related sources which correspond to the inferred signature of enrichment in the source of the MS magmas (López de Luchi et al., 2007). Biotite with Mg / (Mg + Fe^{2+}) between 0.55–0.60 (Iannizzotto and López de Luchi, 2012) was calculated for the LCHPB with the lowest values for the quartz-monzonite-monzogranites of the NW sector. These features indicate a remarkable difference from rocks of similar SiO_2 content belonging to the A2-type Carboniferous granitoids of the Velasco and Famatina Sierras, in which biotite is iron rich (Dahlquist et al., 2010). Therefore, chemical data would suggest arc related sources, high heat flow and probably postcollisional settings. (See Fig. 12.)

7. Discussion

Coeval shoshonite and high-K transalkaline monzonite and granite suites make up the Devonian granitoids of the Sierra de San Luis which were emplaced at the late to post-collisional stage of the Achalian orogeny (López de Luchi et al., 2007). Poor systematic relationships between major and trace elements and SiO_2 contents suggest that monzonite and granite suites result from a combination of magmatic

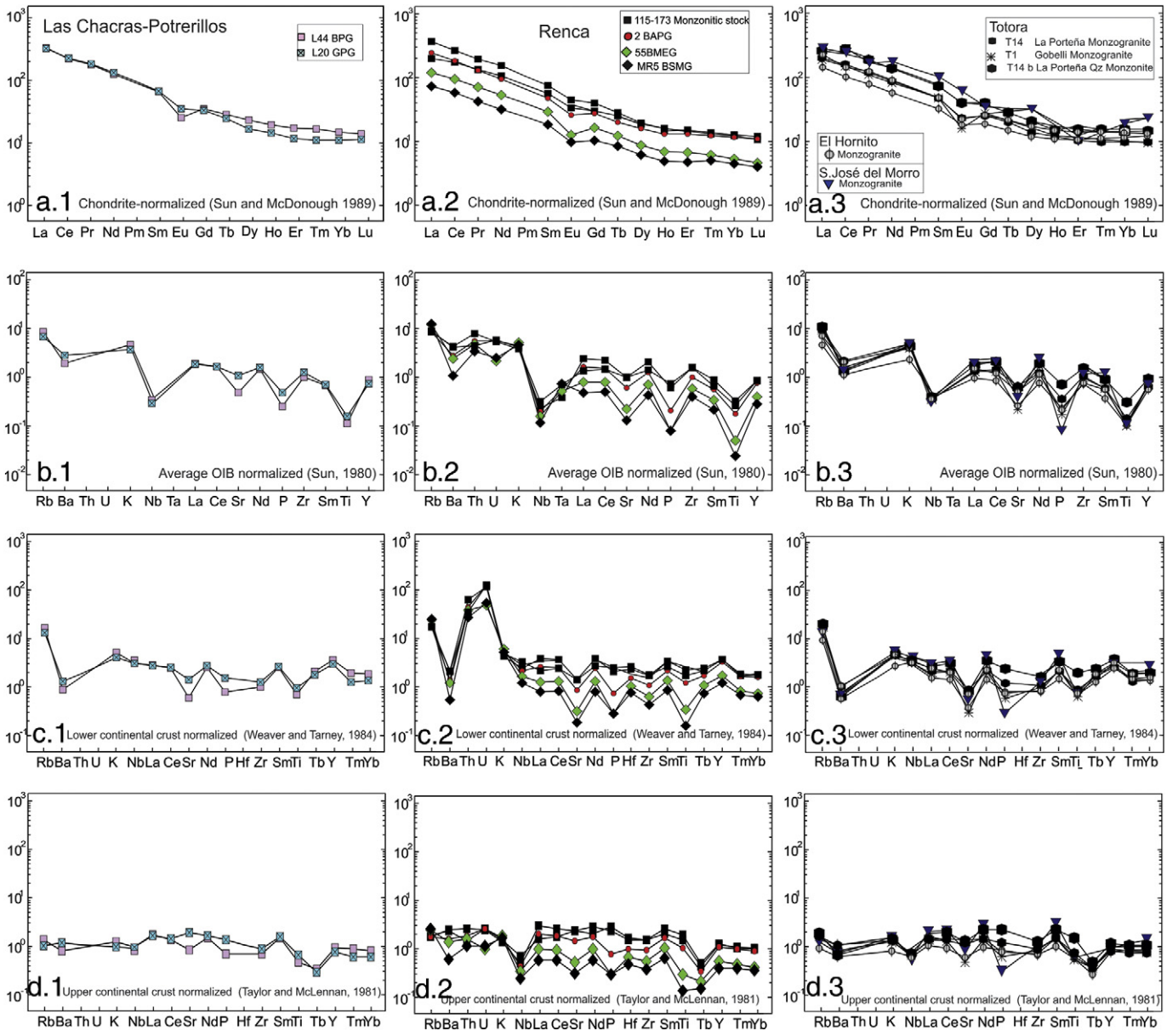

Fig. 8. a) Chondrite normalized REE patterns for representative samples of the monzonite suite and shoshonitic monzogranite (normalized to the values of Sun and McDonough, 1989). Note that trends and SiO_2 increase is accompanied by an increasing europium anomaly are parallel. HREE show a concave upward trend; b) OIB normalized multi-element diagrams (normalized to values of Sun, 1980). Patterns are enriched against up to Ti. Troughs are present at Ta, Sr, Nb, P, and Ti c) LC normalized multi-element diagrams (normalized to values of Weaver and Tarney, 1984) d) UC normalized multielement diagrams (normalized to values of Taylor and McLennan, 1981).

differentiation and mixing/mingling processes involving different magma sources.

7.1. Textural evidence of mingling and mixing between mafic and felsic melts

MMEs are generally considered to have formed by mafic and felsic magma mixing and mingling processes (Barbarin and Didier, 1992; Holden et al., 1991; Vernon, 1984). Mixing takes place either deep in the crust, during the ascent, or even after emplacement by continuous feeding through mafic dikes (e.g., Collins et al., 2000; Weinberg et al., 2001) whereas mingling is commonly a process related with the emplacement or in condition of a marked viscosity contrast. In the studied case the MS would encompass mafic end members, whereas some of the more evolved granites of the GS would represent the felsic pole.

Mafic–felsic mingling and mixing processes occurred at different stages as indicated by several meso- and microscopic features of the porphyritic granites of the GS (López de Luchi, 1996). Type 1 MME, rounded interfaces, finer grain size and diffuse contacts between the MME and the host monzogranite suggest that quenching of mafic magmas played a major role in the generation of the MMEs in a dynamic magma chamber. Rounded, or embayed poikilitic K-feldspar megacrysts compositionally similar to those in the host monzogranite, sometimes mantled by plagioclase occur in Types 1 and 4 MME. Since they are ovoid in Type 1 MME a small rheological difference allowing crystal transportation from the host felsic magma into the mafic magma (e.g. Barbarin and Didier, 1992) is implied. In Type 4 MME K-feldspar megacryst are less rounded, some of them cut across the border which may imply a shorter period of interaction.

Plagioclase shows corroded cores and overgrowth in both the MME and their hosts which suggest mixing and mingling. Smaller scale

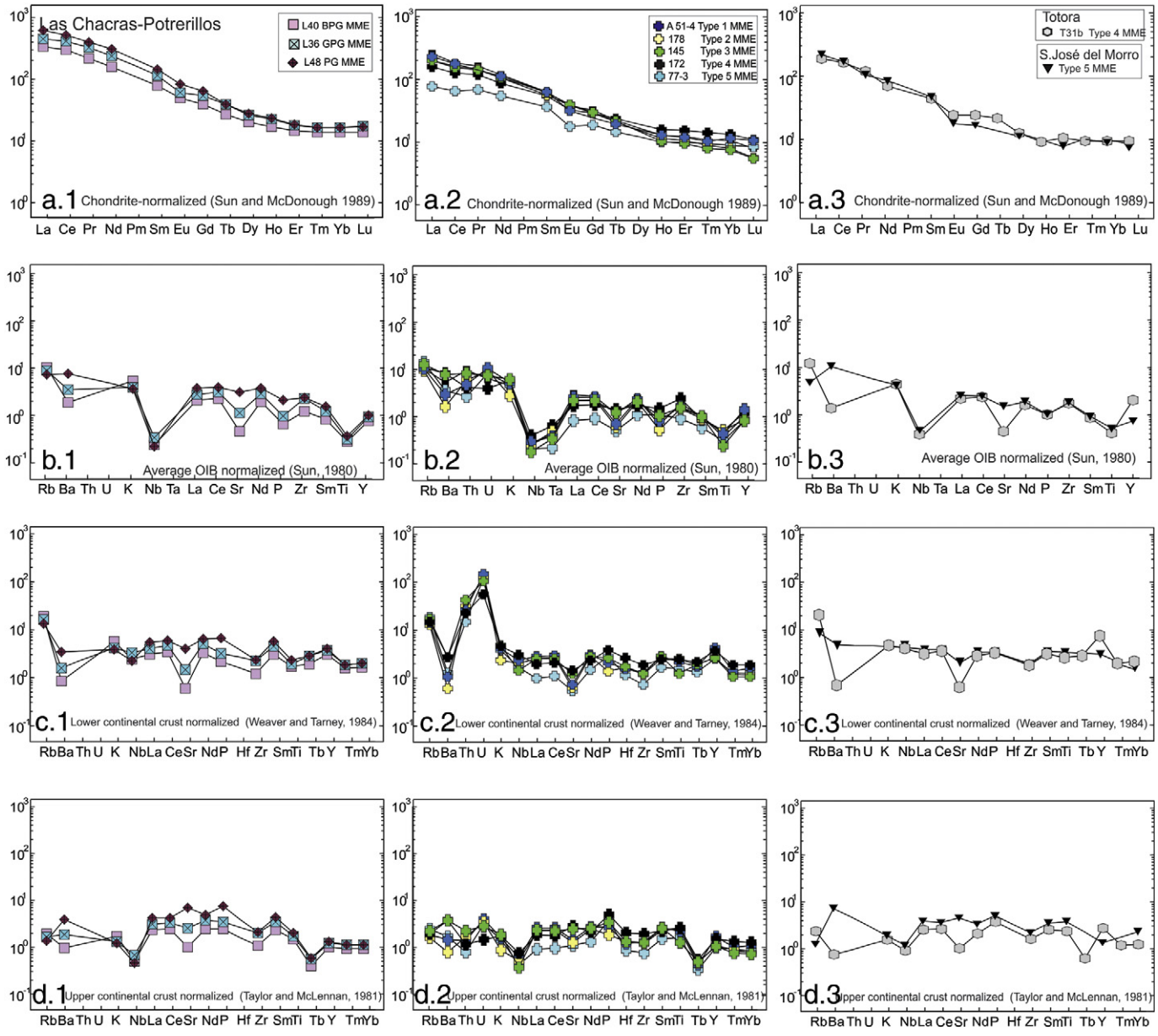

Fig. 9. Multi-element patterns for samples of the MME, A51–4 and 77–3 are vaugnerite being 77–3 the lowest in SiO_2; 145 and 172 are durbachite i.e. the highest K_2O group, and 178, the appinitic-like group which exhibits low MgO and K_2O: a) Chondrite normalized REE patterns. Slopes $(La/Yb)_N$ are lower for 77–3 and 172 whereas, for the appinitic, the slope is slightly steeper; b) OIB normalized multi-element plot. MME are enriched in elements lighter than Nb and show troughs at Nb, Ta, Sr, and Ti. The only difference is in P, which have/has OIB values for the vaugnerite and durbachite and are/is depleted for the appinitic enclaves; c) Upper Crustal normalized multi-element plot. Nb and Tb exhibit troughs, P and U are enriched, but the overall pattern is comparable to the UC, which could suggest that the enrichment of the mantle source is related to subducted sediments. Normalization as in Fig. 8.

evidence of magma mingling is indicated by millimetric clots of mafic minerals in the porphyritic granites and quartz ocelli in the MME. Corroded plagioclase cores and quartz ocelli are distinctly abundant in the aphyric equigranular fine grained Type 3 MME which are richer in SiO_2. Aphyric Types 2 and 5 MME although preserving some corroded plagioclase and scarce ocelli show quenched margins against their host which suggest that they could have been immiscible blebs.

Quartz ocelli indicate a stage of "crystal mush" for the granite when it came into contact with the MS melts. The preservation of the ocelli may suggest fast cooling or ascent since prolonged thermal re-equilibration, readjustment of grain boundaries and late-magmatic to postmagmatic replacement could destroy them. Alternatively the lack of quartz xenocryst would indicate either that the granite magma did not crystallize quartz early in its crystallization history before coming into contact with mafic magma batches or that the mafic magma interacted with a granite that was almost fully crystallized.

7.2. Petrogenesis and sources of the mafic and felsic rocks

Possible petrogenetic processes for the origin of the Devonian monzonite and granite suites can be differentiation of mantle-derived magmas by fractional crystallization, partial melting of a continental crust source triggered by intrusion or underplating of mantle-derived magma or mixing and mingling between coeval mantle and crustal derived melts. The ubiquitous occurrence and predominance of MMEs in more felsic hosts suggests a direct chemical input by mixing and mingling with mantle derived magmas and negligible metasedimentary input, (Barbarin and Didier, 1992; Clemens and Bezuidenhout, 2014; Clemens et al., 2016; Collins et al., 2000; Didier and Barbarin, 1991; Osterhus et al., 2014; Vernon, 1984; Yao-Hui et al., 2006 and references therein). Low $(^{87}Sr/^{86}Sr)_i$ ratios, T_{DM} ca 1 Ga and relatively high $\xi Nd_{(380\ Ma)}$ values preclude significant contamination by older continental crust of the Sierras Pampeanas (Fig. 10a). and imply a source

Table 3
Sr and Nd data for the studied Monzonite and Granite suites of the Devonian granitoids of the Sierra de San Luis. Analysis by mass-spectrometric isotope dilution; 2sigma errors on $^{87}Sr/^{86}Sr$ mostly <0.01 and on $^{143}Nd/^{144}Nd$ <0.005%. TDM1 ages are calculated according to the model of Goldstein et al. (1984). TDM2 ages were calculated according to the model of DePaolo et al. (1991). The calculation of the fractionation index resulted from the equation: $f_{Sm/Nd} = [(^{147}Sm/^{144}Nd)\ sample / 0.1967] - 1$. Data for El Molle pluton were taken from Sato et al. (2001). $(^{87}Sr/^{86}Sr)i$ and εNd(t) values were calculated at t = 380 Ma on the basis of the crystallization ages of the batholiths (Table 1).

	Monzonite suite											
Batholith/Pluton	Las Chacras Potrerillos		Renca					SJMorro	El Molle			
Unit	GPG	Type1MME	ABPM	Type 1 MME	Type 4 MME	Type 2 MME	Type 3 MME	Type 4 MME	Mongabbro	Gabbro	Monzonite	Monzonite
Sample	AH 26	SLC 4	173s	173	35/85	M178	37/85	M02	NG-6*	NG-7*	NG-8*	NG-18*
SiO_2	57.55	54.08	59.78	61.82	54.41	55.01	61.48	49.77				
Rb(ppm)	127	158	189	198	298	176	204	102	67	109	77	96
Sr(ppm)	1299	2996	798	804	334	424	388	1196	1914	1775	3387	2792
$^{87}Rb/^{86}Sr$	0.281748	0.151910	0.376163	0.694831	2.575926	1.197483	1.513753	0.28	0.10121	0.17726	0.06607	0.09945
$^{87}Sr/^{86}Sr$	0.705728	0.704342	0.706496	0.709418	0.720404	0.713479	0.715034	0.7072	0.70722	0.70805	0.70746	0.70738
$(^{87}Sr/^{86}Sr)_0$	0.704203	0.703520	0.704428	0.705559	0.706099	0.706829	0.706627	0.705645	0.706656	0.707061	0.70709	0.706822
Sm	22.57	21.11	17.57	9.04	10.94	10.03	24.92	11.9	12.75	18.5	19.15	16.67
Nd	142.02	145.58	113.35	52.45	62.82	62.08	140.59	65.6	73.86	111.64	141.18	133.95
$^{147}Sm/^{144}Nd$	0.0960780	0.0876635	0.0959976	0.1042512	0.1052633	0.0976876	0.1071515	0.0997	0.1044	0.1002	0.082	0.0752
$^{143}Nd/^{144}Nd$	0.5123122	0.5123330	0.5123075	0.5122772	0.5122730	0.5122357	0.5121613	0.512243	0.512229	0.512225	0.512186	0.512177
$(^{143}Nd/^{144}Nd)_0$	0.5120732	0.5121149	0.5120663	0.5120109	0.5120042	0.5119862	0.5118877	0.5119884	0.511969	0.511976	0.511982	0.51199
eNd_t	−1.47	−0.66	−1.52	−2.44	−2.57	−2.92	−4.84	−2.88	−3.5	−3.4	−3.3	−3.1
$f_{Sm/Nd}$	−0.51	−0.55	−0.51	−0.47	−0.46	−0.50	−0.46	−0.49	−0.47	−0.49	−0.58	−0.62
T_{DM1}	1085	988	1096	1215	1232	1200	1412	1212	1293	1251	1124	1079
T_{DM2}	1247	1181	1254	1333	1344	1373	1529	1305	1367	1342	1262	1223

dominated by a mantle-derived component for the less evolved rocks of the MS, i.e. a juvenile source. Nd isotopic ratios (Table 4) are significantly lower than those of MORB (Fig. 10a). The multi-element patterns (Figs. 8, 9) with troughs in Nb, P and Ti along with high LILE display a clear subduction signature which is consistent with magma sources involving melting of a high field strength element (HFSE)-depleted mantle that has been fluxed by fluids following dehydration of a subducted slab, as observed in modern island-arc environments (e.g. Gamble et al., 1996; Hunen and Allen, 2011).

7.2.1. Sources of the monzonite magma

The different types of enclaves as well as the stocks and syn plutonic dikes suggest no simple model for the production of their respective melt through hybridization of a unique mafic magma batch with a felsic crustal derived magma. Instead, they reflect open-system magmatic processes, involving mixing of melts from different sources and/or at different conditions. The presence of abundant septa of country rocks (Fig. 2a, b), which are sub-parallel to the vertical planar fabric and display a very high aspect ratio (López de Luchi et al., 2004; Siegesmund et al., 2004 and references therein), suggests that the porphyritic granites of the RB and the GPG stocks of the LCHPB were initially emplaced as sheets of low viscosity magmas within the schistosity of the country rocks. Therefore the batholiths would have been constructed from melt-rich magmas injected as sills, by assembly of successive magma batches (Clemens and Mawer, 1992; Petford et al., 1993). The preservation of the overall geometry of the sheet and septa of the country rocks, along with the homogenous lineation and foliation patterns, suggest that no major convective overturn occurred at the scale of the pluton after the emplacement.

Monzonite suite (50–65% SiO_2) stocks, mafic microgranular enclaves, and synplutonic dikes that cover the spectra from monzonite to quartz-monzonite are characterized by low CaO and Al_2O_3, variable TiO_2, high K_2O and K_2O/Na_2O ratio, P_2O_5, transition elements like Cr, Ni, and V, MgO, LREE, Rb, Sr, Ba, Zr and Th, variable εNd(t), and a relatively wider range of $(^{87}Sr/^{86}Sr)_i$. REE are variably fractionated without a substantial Eu/Eu*. Type 1 MME and stocks have similar mineral assemblages and range of whole-rock geochemistry. Coherent negative trends against SiO_2 are shown by TiO_2, Fe_2O_3 (not shown), MgO, CaO, P_2O_5 (Fig. 6) and compatible trace elements which would might suggest fractional crystallization as a dominant mechanism that explains the transition from monzonites to quartz monzonite by the crystallization of amphibole, sphene, biotite, and plagioclase. Y exhibits a negative trend against SiO_2, which suggests amphibole fractionation (Figs. 7a–g.1–3, 8a, b, c.1–3). Nevertheless there is scatter for HFSE, LILE, REE, and Sr which would suggest variable mineral modes. Type 2 MME data exhibits a limited compositional range with high Sr/Y, $(La/Yb)_N$,$(Tb/Yb)_N$ and negligible Eu/Eu*. Type 3 MME are more evolved but also limited in SiO_2 range and are higher than the stocks and Types 1 and 2 MME in SiO_2, MgO, REE_t, La/Yb_N and Tb/Yb_N. Type 4 MME share most of the features with Type 1 or 3 MME (Table 4) but show a distinctly lower $(La/Yb)_N$ and $(Tb/Yb)_N$. Type 5 MME Mg-rich vaugnerites that have high MgO (8.5–9.7 wt%), Cr and Ni (up to 680 and 200 ppm, respectively), show relatively high K_2O (3.5–5%), (Fig. 6a–g.2), Eu/Eu* from 0.7 to 0.9, a moderate enrichment in LILE relative to HFSE, and REE_t up to 300 ppm (Fig. 7a–g.2).

MS stocks, Types 1, 2 and 3 MME (as well as the porphyritic units of GS) high LILE, LREE, Sr, low Yb (c.a. 2) and Sc (<15), positive correlation of La/Yb_N and Eu/Eu* with increasing Sr/Y (30–35 and 0.70–0.85 respectively for 40–90 Sr/Y) coupled with steepness of the REE (La/Yb_N 35–20) pattern and a smooth Eu/Eu*, indicate a relatively deep-seated source with garnet as a major residual phase and a minor role of plagioclase which could imply pressures of 10–12 kbar i.e. 30–40 km crustal thickness (Moyen and Stevens, 2006; Rapp and Watson, 1995). Amphibole is also suggested by the concave-up REE pattern (Fig. 8a.2) of Types 2 and 3 enclaves. Significant lower $(La/Yb)_N$, $(Tb/Yb)_N$ and Eu/Eu* but variable Sr content for Types 4 and 5 MME suggest that melting took place at shallower levels than for Types 1 to 3 MME magmas as well as some cumulatic plagioclase.

The characteristic LILE and LREE-enrichment of the shoshonitic rocks can be attributed to the involvement of an anomalous, amphibole- or biotite-bearing lithospheric mantle domain, enriched in incompatible elements due to mantle metasomatism or the recycling of a metasedimentary component in (paleo-?) subduction zones (e.g. Janoušek et al., 2000, 2004; Jiang et al., 2012; Tatsumi and Eggins, 1995 among others).The high variability of both MgO and K_2O may suggest different degrees of hybridization and/or partial melting and sources whereas variable ratios between HFSE i.e. Zr/Nb might be related to a particular mineral mode or source heterogeneity.

Although the isotopic characteristics of MME are usually not representative of their primary mafic magmas, but might have been substantially modified by mass transfer between enclaves and hosts (Elburg,

	Granite suite												
	Las Chacras Potrerillos							Renca					SJMorro
Monzonite	BPG	BPG	BPG	RG	RG	PG	EG	BAPG	BMEG	BMEG	BMSG	BMSG	MGr
NG-23*	AH 20	SLC 1	SLC 2	SLC 7	SLC 8	PG 1	EG 3	M 60	55	50	57	MR5	M01
	68.22	68.80	71.80	76.00	76.10	70.80	72.80	67.66	71.52	73.45	73.64	75.07	72.16
	196	167	164	403	360	191	301	200	263	234	254	263	196
	356	488	317	34	12	849	516	440	177	128	118	103	301
	1.590303	0.985668	1.483504	34.244697	8.827886	0.651000	1.688000	1.316000	5.310000	5.246019	6.218890	7.341126	1.66101
	0.715079	0.711906	0.716348	0.895143	1.139590	0.707320	0.713418	0.714148	0.737270	0.739209	0.745279	0.751952	0.7154411
	0.706474	0.706573	0.707322	0.709859	1.091826	0.703797	0.704284	0.707027	0.707782	0.707955	0.710743	0.711184	0.706198
20.09	30.56	12.51	8.38	6.07	5.16	9.27	8.03	6.74	5.26	5.21	4.64	2.89	15.6
140.73	173.76	76.05	48.05	23.06	26.42	58.37	51.15	42.88	29.16	28.55	25.85	15.76	82.8
0.0863	0.1063291	0.0994635	0.1054674	0.1591006	0.1232636	0.0960000	0.0949000	0.0951000	0.1090809	0.1102737	0.1084545	0.1107052	0.114
0.512197	0.5122583	0.5122395	0.5122386	0.5123733	0.5123875	0.5123160	0.5122420	0.5122260	0.5122436	0.5122256	0.5122131	0.5122162	0.512252
0.511982	0.5119937	0.5119920	0.5119761	0.5119774	0.5118086	0.5120740	0.5119990	0.5119890	0.5119651	0.5119440	0.5119361	0.5119334	0.5119609
−3.2	−3.02	−3.06	−3.37	−3.34	−6.64	−1.32	−2.66	−3.10	−3.33	−3.74	−3.90	−3.95	−3.71
−0.56	−0.46	−0.49	−0.46	−0.19	0.18	−0.51	−0.52	−0.52	−0.45	−0.44	−0.45	−0.44	−0.42
1149	1265	1214	1282	2160	−6285	1079	1165	1197	1319	1361	1355	1380	1371
1279	1373	1376	1401	1395	1708	1239	1352	1378	1406	1439	1452	1456	1456

1996; Holden et al., 1991; Pin et al., 1990), Types 2, 3 and 4 MME show rather uniform ($^{87}Sr/^{86}Sr$) independently of their host whereas εNd(t) decreases as SiO_2 increases being Type 3 the lowest in εNd(t).On the contrary Type 1 MME and stocks depict continuous trends for these ratios which suggest hybridization.

Source heterogeneities and or involvement of lower crustal segment could explain these trends. An enriched mantle source is proposed for Type 1 MME and stocks whereas probably a lower crustal one with higher residence time or a highly hybridized source that underwent different degrees of partial melting which yielded at lower degrees relatively silica enriched melts like those corresponding to Type 3 MME. Apatite saturation temperatures (1000–1040 °C, Table 4) would support this possibility.

As the monzonitic (57–65% SiO_2) stocks of the LCHPB and RB are isotopically more primitive (Tables 3, 4, Fig. 10a,b,c) than any of the MME or syn-plutonic dikes of the rest of the Devonian plutons except for PG and one if its MME and EG, therefore the stocks should be closer to the composition of the mafic end member.

At a similar SiO_2 content Types 2, 3 and 4 show higher $(^{87}Sr/^{86}Sr)_i$ and more negative εNd(t) than the stocks and Type 1 MME (Tables 3, 4) which suggest that they could represent a distinct source. High MgO, CaO, Cr and Ni but LILE and LREE contents similar to those of the more evolved rocks may suggest that Type 5 represents higher degree of partial melting of an enriched mafic source. The more mafic monzogabbro Type 5 MME have high TiO_2 and HFSE contents and their Ta/Yb ratios (0.5) are significantly higher than E-MORB (0.2), suggesting a rather fertile mantle source (Pearce et al., 2005).

Contribution of a subduction component is indicated by the high ratio of LILE and LREE to HFSE (Fig. 7a–g.1–3). and the negative Nb–Ta or Nb anomalies (Fig. 9b, c, d.1–3) that is exhibited by the MS rocks. The subduction-related component can be either a slab-derived fluid or melt. Fluids released from the subsolidus dehydration of the subducting slab are the principal carriers of incompatible elements and promote metasomatism of the mantle wedge (Tatsumi and Eggins, 1995). Slab-derived fluid is enriched in highly mobile elements (e.g. Rb, Cs, Ba, U and Pb) and partial melting of a mantle metasomatized by such a fluid would produce magmas with high Th/Ta ratios (Pearce et al., 2005). All the MS rocks of the RB have Th/Ta ratios above 4 higher than that of primitive mantle (Th/Ta = 2.1, Sun and McDonough, 1989). Significant assimilation of crustal melts can be precluded in the more mafic rocks since the available isotopic data for the less evolved mafic MME of PG is primitive $(^{87}Sr/^{86}Sr)_i$ 0.70352 and εNdt −0.66 and combined with LILE and LREE enrichment.

Therefore the mafic end members of the MS would have resulted from partial melting of relatively fertile mantle (OIB like) at a deep level, probably induced from astenospheric upwelling during a postcollisional stage. The mantle source of the most primitive magmas must have been characterized by a significantly lower $^{143}Nd/^{144}Nd$ relative to the primitive mantle (De Hollanda et al., 2003; Florisbal et al., 2009). A gradually shallowing of the sources is indicated by the Type 4 MME and dikes as well as Type 5 MME magmas by lower Sr, $(Gd/Yb)_N$ and $(La/Yb)_N$.

7.2.2. Source for the granite suite

Based on the linear variation of TiO_2, Al_2O_3, Fe_2O_{3t}, MgO, CaO, K_2O, P_2O_5, vs. SiO_2 (Fig. 6), the granites of the GS can be interpreted as fractionation product of mafic magmas. Nonetheless, the distinct rock types form distinctive groupings on Sr, Ba, Y, Nb vs. SiO_2 (Figs. 6 and 7), which can be best accounted by fractional crystallization as well as by the partial melting of distinct sources.

The aluminous to weakly peraluminous, magnesian alkali calcic to calc–alkaline biotite amphibole porphyritic granitoids (65–73% SiO_2) straddle the fields of the shoshonite and high K calc–alkaline series (Rickwood, 1989) (Fig. 4a). Its alkalic and mildly peraluminous character might be associated to different sources, anatexis of a lower crust hornblende-rich source (Whitney, 1988) mixing of crustal-derived melts with the enriched or mantle-derived monzonitic melts. Monzonite suite stocks and the porphyritic GS rocks broadly contain the same mafic minerals, Mg–hornblende, Mg–rich biotite, magnetite, titanite, and apatite in different modal amounts (Iannizzotto and López de Luchi, 2012).

Fractional crystallization of the granites from vaugneritic hybrid stocks magmas would account for the continuous linear trends in TiO_2, Al_2O_3, Fe_2O_{3t}, MgO, CaO, K_2O, P_2O_5 vs. SiO_2, the parallelism of the REE-normalized patterns (Fig. 8a.1–3) and the lack of a prominent compositional gap from the monzonite to quartz-monzonites of the MS to the porphyritic granitoids of the GS. Fractionation of biotite, apatite and titanite is indicated by negative anomalies for Ba, P, and Ti (Fig. 8a.1–3), respectively, whereas negative anomalies in Sr and Eu indicate plagioclase and Y negative peak and its negative correlation with SiO_2 indicate amphibole (Fig. 7f). REE_t decrease with increasing SiO_2 (Fig. 7e) is also related to the important role of titanite and apatite

Table 4
Diagnostic chemical and isotopic features of the Monzonite suite rocks. Methods as indicated in Table 3 and methodology.

Unit	Las Chacras Potrerillos				Renca						Totora			SJMORRO
	Stock	MME			Stock	MME					Stock	MME		MME
	GPC	Type 1			ABPM	Type 1	Type 2	Type 3	Type 4	Type 5	Monzonite	Type 4		Type 4
Host		BPG	GPG	PG		BAPG	BAPG	ABPM	BAPG/ABPM	ABPM		Monz. Stock		Monzonite
SiO_2(%)	57.55–65	57.77–62.02	58.04–60-06	51.41	58.49–62.68	55.01–63.43	54.26–55.01	60.47–61.48	54.09–58.53	45.92–50.34	61.22–63.93	55.65		49.77
MgO(%)	1.4–2.8	2.99–3.29	3.54–3.7	4.01	2.2–4.11	2.02–3.02	3.03–3.46	4.77–5.82	5.01–6.55	8.54–9.69	1.32–3.03	3.95		8.03
K_2O(%)	4.26–6.01	3.78–6.36	4.29–4.42	4.16	2.85–4.81	4.02–6.4	2.77–4.57	5.28–6.46	5.23–7.32	3.32–4.68	4.83–6.01	5.05		4.72
Cr (ppm)	20–60	80–120	90–120	ND	40–230	60–130	80–120	90–140	240–360	530–680	10–64	50		ND
Eu/Eu*	0.7–0.8	0.7–0.8	0.7	0.8	0.6–0.8	0.7–0.9	0.8–0.9	0.8	0.6–0.9	0.6	0.7–0.8	0.6		0.6
$(La/Yb)_N$	24–37	20–23	21–25	35	10–24	20–22	20–27	26–31	10–18	10–14	15–27	9		15
$(Tb/Yb)_N$	1.94–2.28	1.67–1.78	1.98–2.23	2.26	1.4–2.13	1.2–1.9	2.3–2.5	2.8–3	1.5–2	1–1.6	1.84–2.44	1.09		0.7
REE$_t$(ppm)	280–360	350–370	380–490	620	160–370	150–490	120–320	310–680	180–320	145–300	320–340	450		380
TApSat*	950–1060	920–960	980–1000	1000–1070	900–1000	910–970	770–870	1000–1040	930–1090	880–910	980–1020	970		880
$(^{87}Sr/^{86}Sr)_0$*	0.704065–0.704526	0.705623	0.703551	0.70352	0.704428	0.705559	0.706829	0.706627	0.706099					0.704645
$T_{DM\ 1}$	1085			988	1096	1215	1200	1412	1232					1112
$T_{DM\ 2}$	1247			1181	1254	1333	1373	1529	1344					1205
$\varepsilon_{Nd(380)}$	−1.47			−0.66	−1.52	−2.44	−2.92	−4.84	−2.57					−1.48

in the differentiation process. The Sr/Y ratios of the porphyritic granitoids are positively correlated with SiO_2 (not shown) due to amphibole fractionation which also controlled the increase of La/Yb_N (Fig. 7g.) and explain the concave-upward chondrite-normalized REE patterns. López de Luchi et al. (2007) proposed that preservation of anorthite rich corroded plagioclase cores, clots of mafic mineral and abundant MME suggest mingling but fractional crystallization would be also important as a controlling process because normal zoning with more sodic external zones and rims are observed together with oligoclase in the groundmass of the porphyritic granitoids.

Nevertheless progressive hybridization between the vaugneritic magma and a granite anatectic magma is suggested by the linear trend of $(^{87}Sr/^{86}Sr)_i$ and εNd(t) vs SiO_2. Low Rb/Sr ratios (0.28–0.58) would rule out an origin from a mafic magma by extensive fractional crystallization. Therefore, we consider that the porphyritic granitoids are derived from lower crust magmas hybridized with the magmas from which the MS stocks of the RB originated. Since the isotopic data, i.e. $(^{87}Sr/^{86}Sr)_i$ (0.706474–0.707322) and ε_{Ndt} − 3.07 to −3.37 are less radiogenic than those of the MS stocks they might have fractionated at a large scale from hybrid magmas at depth. Similar processes have been extensively modeled (e.g. Ferré et al., 1998; Huppert and Sparks, 1988; Jiang et al., 2012; Kemp, 2003; Petford and Gallagher, 2001).

Biotite muscovite granites or biotite equigranular monzogranites (SiO_2, 71 to 73%) of the RB, LT and SJMP are magnesian, alkali calcic and metaluminous to weakly peraluminous (Fig. 4) and have low MgO, Cr and Ni, variable K_2O and Na_2O (Fig. 6). The mineral assemblage of the biotite muscovite granites consists plagioclase, biotite, muscovite and K-feldspar with minor zircon, Fe–Ti oxides and apatite. The restricted SiO_2 range prevents from evaluating trends. Compared with the porphyritic granites they show high Al_2O_3, K_2O and Rb/Sr, and low CaO, P_2O_5, Sr, and REE_t. $(^{87}Sr/^{86}Sr)_i$ higher than for the porphyritic granites and slightly more negative εNd(t) indicate that their parental magma is derived from a crustal source. RG of the LCHPB magmas as well as the biotite syenogranites of RB and some of the monzogranite of the SJMP are characterized by higher SiO_2, K_2O/Na_2O, Al_2O_3/TiO_2, Rb and Rb/Sr >2 ratios, and more pronounced negative anomalies in Ba, Nb, Sr, Eu and Ti. Besides, they display low $(La/Yb)_N$ <10, Sr/Y and slightly more negative εNd values (−4), and slightly higher Nd model ages (1.36–1.38 Ga). The Sr/Y ratios are not correlated to SiO_2 which might suggest that plagioclase was stable at the source. Their variable Al_2O_3/TiO_2 ratio from 50 to 200 might correspond to variable amounts of Ti bearing phase in the source. The geochemical features (high Rb/Sr ratios and contents of K_2O and SiO_2) are consistent with derivation from a felsic micaceous crustal source (cf. Jung and Pfander, 2007; van de Flierdt et al., 2003) or could correspond to low degree of partial melting of an unexposed lower crust mafic source as it is suggested by the isotopic signature which does not fit that of the Early Paleozoic metaclastic rocks of the Sierras Pampeanas. RG show enrichment in Nb and Y, plot in the WPG field and are A2 type granites.

7.2.3. Sources of the PG and EG of the Las Chacras Potrerillos batholith

The alkali calcic weakly peraluminous magnesian shoshonite series (67–72% SiO_2) porphyritic and (72–73% SiO_2) equigranular granites of the LCHPB exhibit overall major element trends similar to those of the above described porphyritic granitoids but they are poorer in CaO and richer in Sr, Ba and Zr. Their extremely low Rb/Sr (Fig. 7k.1) does not support an origin by fractional crystallization. The PG show distinct compositional trends from the other rock types of the GS suggesting that they were not produced by fractional crystallization of same mafic magma source than the porphyritic granitoids or by simple mixing between a mafic magma and a more felsic magma (e.g. the biotite granite). The Sr–Nd isotope compositions of the PG are consistent with those of mantle-derived magmas since they are the less evolved signatures among the studied rocks except for the MME that it contains.

PG are characterized by variable Na_2O, Al_2O_3, low CaO and high Rb, Ba,Sr, and relatively high Sr/Y Although negative correlations of MgO

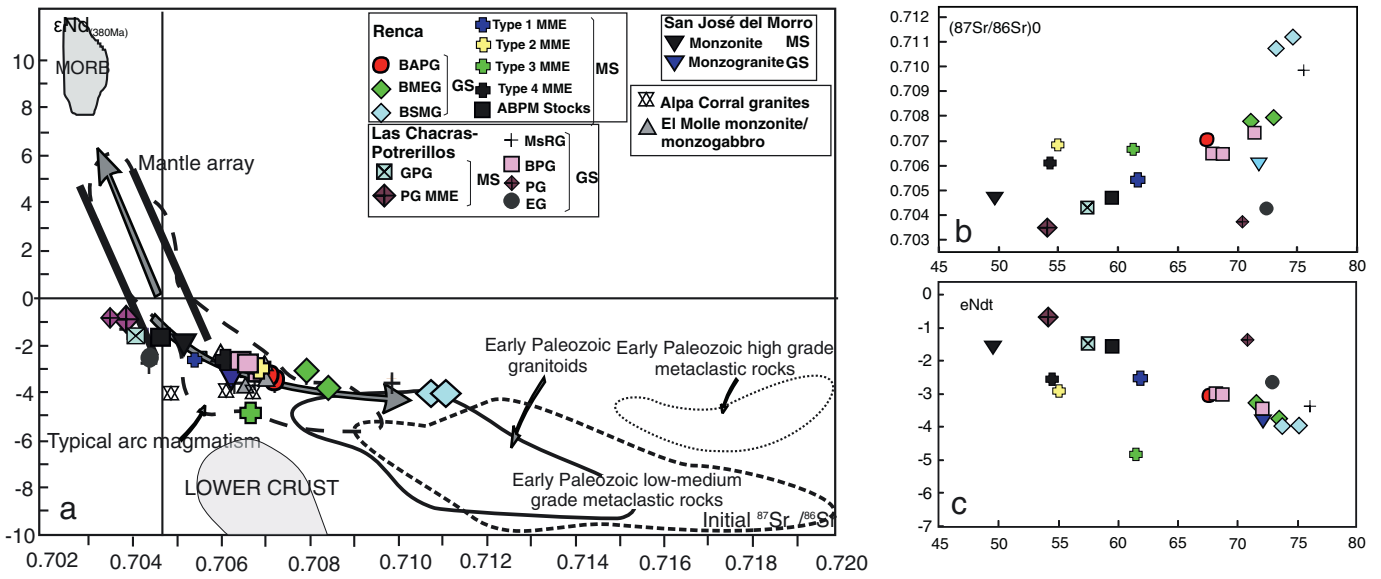

Fig. 10. a) $\varepsilon Nd_{(380)}$ vs $(^{87}Sr/^{86}Sr)_i$. Participation of a component with εNd higher than those of the Sierras Pampeanas average crust is required to explain the Nd isotopic composition of the Las Chacras-Potrerillos, Renca, and S. José del Morro granite suites monzogranite and quartz-monzonites which are located in the shoshonite field in the K_2O vs. SiO_2 plot. Data suggest juvenile input into the crust since they are considerably younger than the 1.8–1.6 Ga crustal residence age interval for the Eastern Sierras Pampeanas (Steenken et al., 2004, 2011); b) $(^{87}Sr/^{86}Sr)_i$ vs SiO_2; c) $\varepsilon Nd_{(t)}$ vs SiO_2.

and P_2O5 vs SiO_2 could be explained by fractionation crystallization K_2O, Na_2O, Al_2O_3, Rb, Sr, Zr, Ba show scattered trends versus SiO_2 (Figs. 6, 7) which are most probably controlled by either plagioclase fractionation at the emplacement level or variable proportions of residual plagioclase in the source or cumulates. Although we lack REE data high Sr/Y (30–50) similar to that of MS stocks like GPG of the LCHPB, might suggest a deep seated source. Their Sr/Y shows no correlation with CaO, suggesting source inheritance or cumulatic plagioclase. Under conditions of fluid-absent melting, plagioclase stability is strongly pressure dependent (Moyen and Stevens, 2006) being gradually consumed at pressures >10 kbar. Both the zircon (~800 °C) and apatite (~960 °C) saturation temperatures are sufficient for the onset of fluid-absent dehydration melting of amphibole (~820–900 °C) (Moyen and Stevens, 2006). Thus, we suggest that the PG were most probably generated by melting of enriched mantle mafic rocks under fluid absent conditions. Nevertheless high Sr suggest some cumulatic plagioclase since experimental E-MORB melting at ca 12 kbar and 800–900 °C generates magmas with 400–500 ppm of Sr (Zhang et al., 2013).

EG shares most of the features of PG but their limited SiO_2 interval 72–73% precludes the analysis differentiation process. Anyway their Rb/Sr >1 suggests fractionation of plagioclase from a melt probably equivalent to that of PG. Available cooling ages of PG and EG (Table 1) suggest a common cooling history with the MS stock, GPG. We assume that the PG-EG represent a melting event of the enriched mantle with limited hybridization with crustal melts due to a short residence time at the melting site probably related with a faster ascent rate.

7.3. Geodynamic setting

Middle to Late Devonian batholiths which intruded the basement of the Eastern Sierras Pampeanas (López de Luchi et al., 2004, 2007) are located along a belt almost parallel to the trend of the Ordovician Famatinian orogen (Grosse et al., 2008).

The large volume of the Devonian granitoids always associated with mantle derived mafic rocks (López de Luchi et al., 2004, 2007 and references therein) points to abnormal thermal gradients and fertile lower crustal sources. Liquidus temperatures calculated from the apatite saturation thermometer indicate temperatures between 900 and 1080 °C for Monzonite Suite rocks and between 800 and 1020 °C for the GS rocks. An enriched mantle source is supported by the rather young T_{DM}, high $(^{87}Sr/^{86}Sr)_i$, relatively radiogenic εNd(t) i and high LILE and LREE in the more mafic rocks. Subduction zones along the Proto-Pacific margin of Gondwana predated the Devonian convergence that ended c.a. 390 Ma with the collision of the Chilenia microplate (Willner et al., 2011 and references therein). Tectonic discrimination diagrams (Harris et al., 1986; Pearce et al., 1984) suggest a volcanic arc setting which could be either an inherited signature or imply an active/recent subduction.

Recent numerical models of convergent margins (Currie et al., 2007) indicate that the buoyant subducted sediments detached from the subducting plate at 100 km depth led to a subhorizontal sediment plume that intrudes the continental lithosphere. Horizontalization of the subducting plate controlled the migration of the magmatic front inboard the active margin. The onset of lithospheric destruction and thinning beneath Early Paleozoic crust may have occurred as a result of post-collisional subducting slab detachment. With detachment of the oceanic part of the subducting slab, hot astenospheric mantle rises up through the lithospheric gap and causes a transitory thermal anomaly in the mantle wedge. In this scenario, different sources could have contributed to the construction of the batholiths and plutons from partial melting of the previously enriched mantle, i.e. the shoshonite suite, crustal derived melts with intraplate signature like the RG of the LCHPB, a part of the granite suite, and probably even astenospherically-derived magmas that could correspond to the lamprophyres that are spatially related to the Devonian granitoids (López de Luchi et al., 2004, 2007). A postcollisional context and the Cordilleran affinity that is exhibited by the MS rocks and most of the GS rocks could match an origin of the Devonian granitoids as products of slab-break off (Davies and von Blackenburg, 1995) with mantle and/or crustal melting triggered by astenospheric upwelling through slab window. Since this magmatism occurred immediately after the collision of Chilenia (Willner et al., 2011 and references therein) and is associated with adiabatic decompression as indicated by the shallowing of the sources, slab failure is a reasonable scenario (Hildebrand and Whalen, 2014).

The presence of an external stress field, even if a weak one, may have favored contamination and hybridization (Schaltegger and Brack, 2007) between coeval granitic and mafic magmas, as well as provided conduits for mafic magmas arising from the previously-enriched mantle

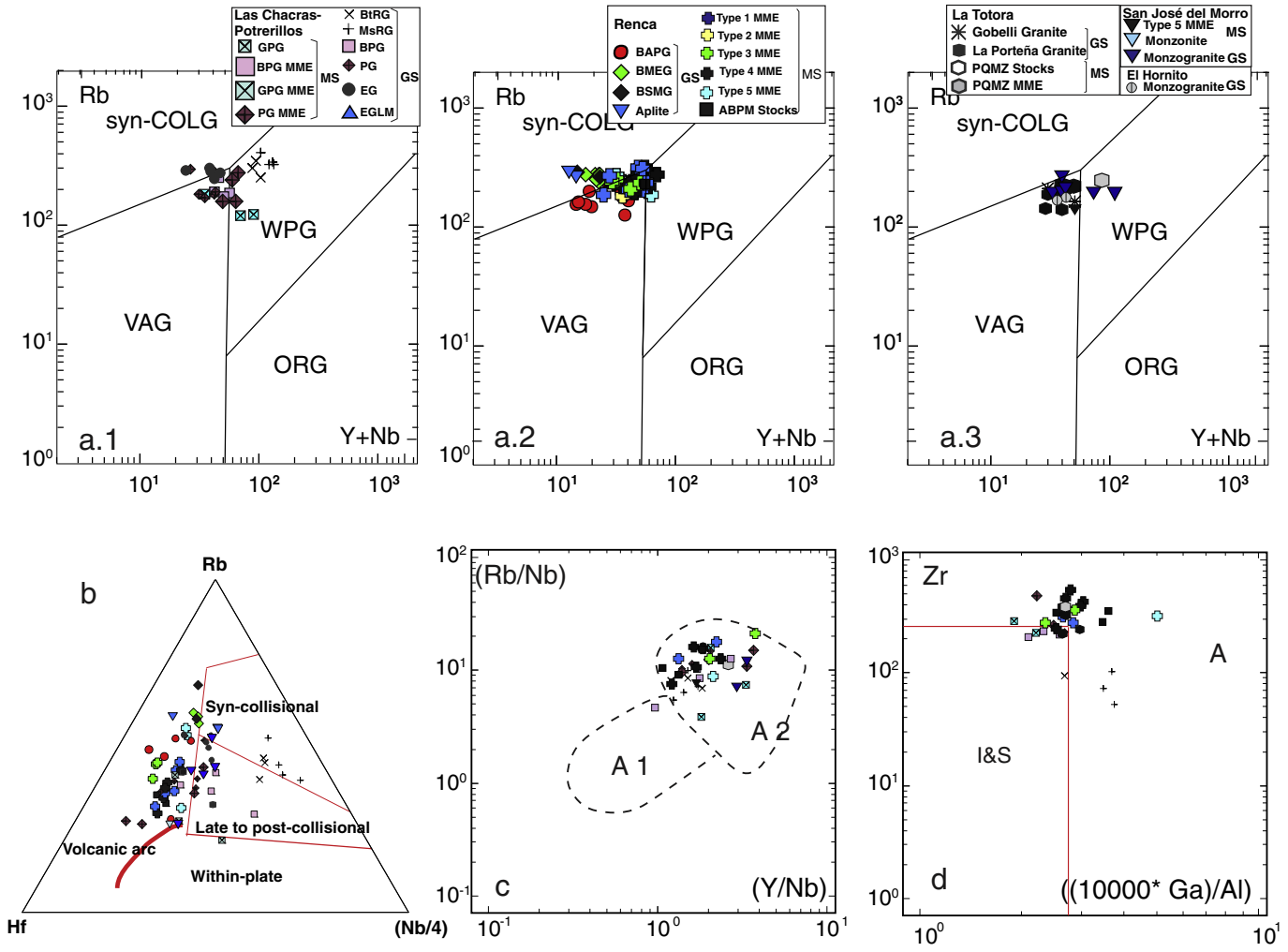

Fig. 11. Petrotectonic plots. a.1–3) Rb vs Y + Nb plot(Pearce et al., 1984). Note that only RG granites of the LCHPB (a.1) and two monzogranites (a.3) of the SJMP plot in the within plate granite field (WPG). The lack of Ga data for the latter preclude their inclusion in plot d. The rest of the samples that plot in WPG field are MME. Abbrev.: VAG: volcanic-arc granites, Syn-COLG: syncollisional granites, ORG: ocean-ridge granites; b) Hf–Rb/30–Nb/4 plot (Harris et al., 1986). Most of the samples plot in the volcanic arc field.; c) Rb/Nb vs Y/Nb plot (Eby, 1992), d) Zr vs Ga/Al (Whalen et al., 1987). In both diagrams only the samples that are located in the WPG granites are included.

and controlled the ascent. The oldest age, 393 Ma, which corresponds to the BAPG of the RB, is almost coeval with the inferred time of the collision of the Chilenia plate with the margin of Gondwana (Willner et al., 2011). At a regional scale, the emplacement of the Devonian batholiths of San Luis took place contemporaneously with the activity of NNW–SSE sinistral transtensional and NNE–SSW strike-slip shear zone systems (Sims et al., 1998) that led to a NNE–SSW-directed extension (Fig. 1), allowing the formation of magma conduits (López de Luchi et al., 2004, 2007, and references therein). Cooling and exhumation could be related with the latest record at 375 to 351 Ma of the activity of the NNE Río Guzman shear zone.

A model is proposed in which astenospheric underplating of the lithosphere induced limited partial melting of the enriched lithospheric mantle which first generates LILE and REE enriched high T granites like PG and EG and as melting proceed high mafic hydrous magmas like those represented by the MME of the PG facies of the LCHPB. These magmas were emplaced in the lower crust, differentiated by fractional crystallization and hybridization with acidic melts derived from the low degree of partial melting of the lower crust by both heat input and the introduction of water released upon adiabatic decompression. Variable degrees of hybridization originated parental magmas to the monzonite stocks and Type 1 MME. The crustal derived magmas would be equivalent to the magnesian and alkali calcic SiO_2 rich granites BMSG, BSMG or the Gobelli Granite. Curved array in the εNdt vs $(^{87}Sr/^{86}Sr)_i$ diagram (Fig. 10a) suggests mixing processes. Positive correlation between $(^{87}Sr/^{86}Sr)_i$ and SiO_2 suggests either mixing or AFC processes whereas the relatively less pronounced εNdt variation may suggest some source heterogeneity. Protracted residence at the lower crust favored differentiation by fractional crystallization of the hybridized magma that originated parental magmas of the porphyritic high-K quartz monzonite-monzogranite. Based on the available ages the older rocks correspond to the isotopically less evolved facies, i.e. PG and EG of the LCHPB and the Monzonite stock of the RB which slightly predated the emplacement of BAPG of the RB and BPG; GPG and Type 1 MME magmas would have crystallized slightly later. Almost coeval ascent of these different hybrid magma batches in the crust was probably favored by pre-existing crustal scale discontinuities. Melt pods of the monzonitic magmas (Type 1 MME) were injected in the high-K quartz monzonite–monzogranite and underwent mechanical mingling and probably diffusive exchange with their host as they coalesced. Melts derived from a mafic lower crust were intruded into the porphyritic quartz monzonite–monzogranite as Type 2 MME. Type 3 MME represent a particular hybridized melt since it is isotopically more evolved but rich in MgO and REE_t which suggest a mafic source. Lower P melting of the enriched mantle source and/or a mafic lower crust will generate the parent melts that were emplaced in the crystallizing previous units as synplutonic dikes that disaggregated as Type 4 enclaves. Finally bubbles of a more primitive MgO rich magma that quenched in the cooling

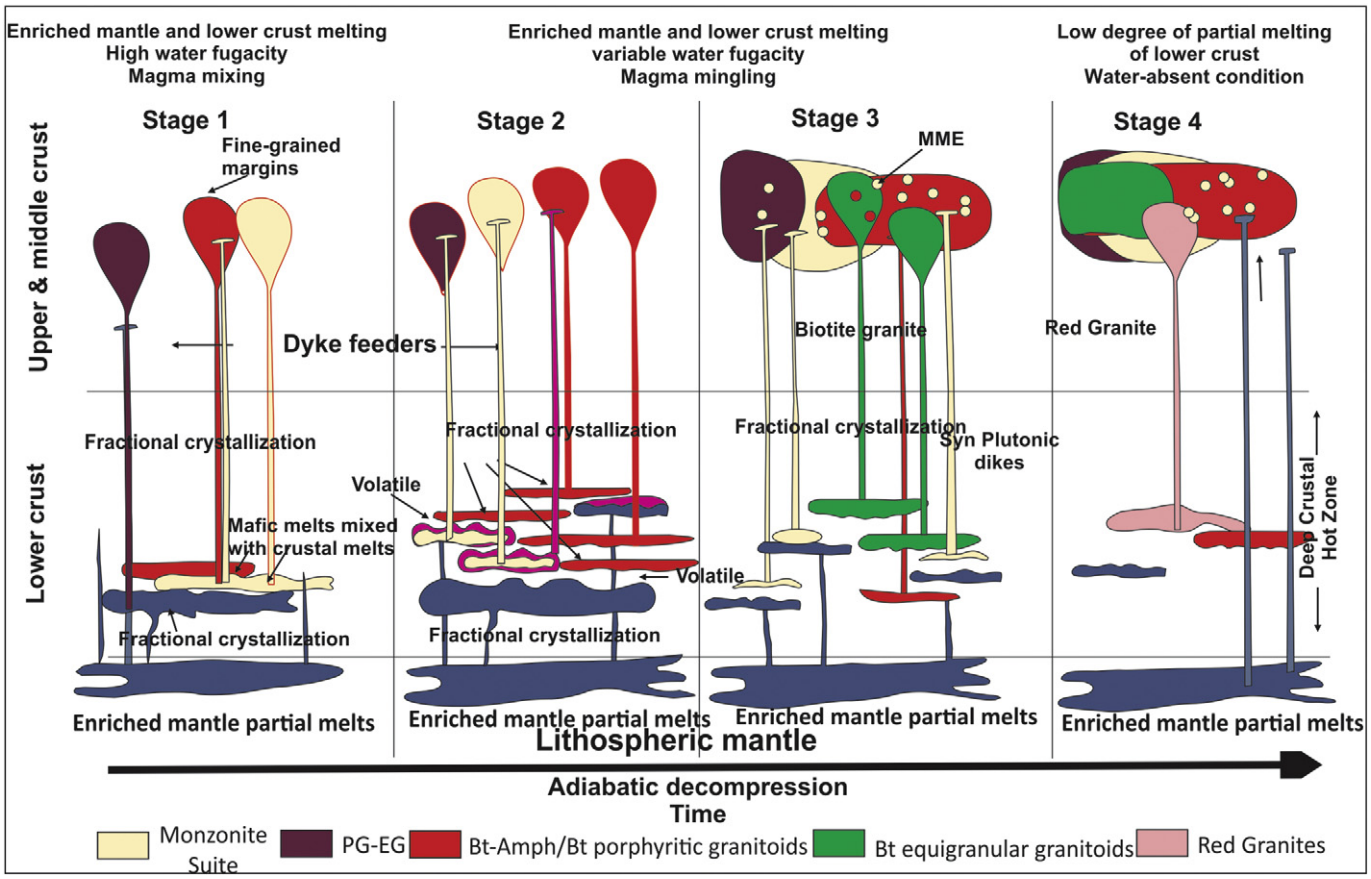

Fig. 12. Schematic summary (modified after Luo et al., 2015) of the sources and processes controlling the evolution of the Monzonite and Granite suites. Stage 1: enriched mantle and mafic lower crust melting and mixing at the source. The hybrid magma is the source of the stocks of the Monzonite Suite whereas the mafic lower crust is the source of the porphyritic facii of the Granite Suite. Stage 2: continuous melting of the lower crust at variable water fugacity led to the assembly of the porphyritic granitoid facii whereas hybrid magma were injected into the partially crystallized previously emplaced units. Stage 3 discrete lower crust magma batches generated under variable fluid conditions were emplaced as the equigranular biotite granites. Stage 4. low degree of partial melting of a portion of the lower crust under lower P conditions related with adiabatic decompression. The higher Ga/Al of these rocks is an indication of plagioclase being a stable phase at the source.

porphyritic granitoids of the GS are represented by Type 5 aphyric MME. The protracted period of multiple, mafic intrusions allowed temporary overstepping of biotite- and/or muscovite-incongruent melting reactions that finally led to the more evolved A2-type RG of the LCHPB. Adiabatic decompression is indicated by progressive lower $(La/Yb)_N$ shown by the synplutonic dykes that intruded a still warm but almost fully crystallized porphyritic monzogranite, the Type 4 derived from them and the quenched magma blebs that made the Type 5 MME. Biotite cooling ages are older than 350 Ma except for the RG which shows Carboniferous ages. These granites exhibit A-type signature that is considered as a hallmark of the Late Devonian (365–370 Ma) Achalian magmatism (Rapela et al., 2008). Therefore magmatism from the Early to Middle Devonian recorded an episode of crustal growth by the input of enriched mantle derived magma which would lead to partial melting of and mixing with lower crustal sources. Repeated recharge of the magma chamber and combined uplift would lead to restricted mixing and to the ascent of discrete magma batches. Their interaction at the level of emplacement would lead to mingling or at the latest stages to the quenching of mafic blebs like the Type 5 MME.

8. Conclusions

MS rocks correspond to a shoshonite transalkaline series and are metaluminous alkali–calcic and magnesian, whereas, the granite suite rocks are transalkaline-to-subakaline mostly mildly peraluminous alkali–calcic and magnesian monzogranites. Only a small group of EG and the RG of the LCHPB are ferroan. The MS rocks are mostly vaugnerites with minor appinite and durbachite among the enclaves. The shoshonite affinity of the MS rocks suggests that melting of a previously-enriched layer of subcontinental lithospheric mantle that was probably metasomatized by a subduction component probably predating the 390 Ma collision of the Chilenia microplate. An important episode of crustal growth by juvenile magma input is indicated by T_{DM} (one stage) between 1.0 and 1.1 Ga which is considerably younger than the Eastern Sierras Pampeanas background of 1.6–1.8 Ga. An important fact is that the isotopic signature of the inferred felsic pole does not match that of the different older metasedimentary crustal rocks of the Sierras Pampeanas. Therefore this felsic end member might represent a partial melt of either an igneous source, mixing of juvenile and older material that give rise to a distinct T_{DM} or alternatively of a different and unexposed mafic crustal source.

GS encompass rocks that underwent different processes and, consequently, granitoid sources are more difficult to constrain. Their parental magma might involve mixing of crustal-derived melts with the enriched, mantle-derived monzonitic melts, melts derived through fractionation of the monzonitic magmas, and melts derived from a lower crustal source. In any case, deep-seated interactions between felsic and mafic magmas could have been responsible for the common characteristic of the MS and most of the GS rocks. This implies that some differentiation occurred before magma emplacement, either in deep-seated intermediate chambers or in magmatic conduits. At the emplacement level mafic-felsic magma interactions were limited to mingling between mafic pulses and partially crystallized granites.

Mixing occurred between lower-crust anatectic melts and water-bearing enriched mantle derived magmas that invaded the crustal source region before melting and granite generation. Water released upon adiabatic decompression could have favored extensive melting of crustal segments. This interaction generated the first batch of shoshonitic monzonite magmas that are the source of the stocks and Type 1 MME. Hybridization of this already mixed melt with the felsic lower crustal derived magmas generated the porphyritic granitoids of the granite suite. The low Rb/Sr (<1.2) in the shoshonitic granitoids is not consistent with an origin of extensive fractional crystallization from a mafic parent. Low melting percentage of the enriched mantle generated PG and EG facies. The highly-evolved high-K biotite equigranular granites represent pure lower crustal melts. Multiple intrusions of the monzonitic, water-bearing mafic magmas, distributed over a protracted period of time, may have invaded the lower crustal source and triggered partial melting by the temporary overstepping of incongruent melting reactions into a pre-heated crust. At the waning stages of these processes limited hybridization led to Type 4 MME and synplutonic dikes and to the high Nb–Y RG. The scarce MgO rich Type 5 MME are quenched mafic melts probably directly derived from the enriched mantle source.

Middle Devonian postcollisional granitoid emplacement was localized in a belt parallel to the trend of the previous orogenies which may suggest that it was controlled by structures related to major crustal discontinuities. The transition from thrust to transcurrent-related tectonics may have played an essential role in the ascent of mantle-derived magmas and may have facilitated their interaction with the crustal melts which seem to be to a large extent the products of reworking of an unexposed crustal source. As a whole this post-collisional magmas reveal mantle-derived contributions.

Supplementary data to this article can be found online at http://dx.doi.org/10.1016/j.lithos.2017.05.018.

Acknowledgments

This research was partially funded by the PICT'97, ANPCyT 97 07-00000-00539 and the International Cooperation Project of Antorchas-DAAD 13740/1-87. We are grateful to the German Science Foundation (DFG) for Grants Si 438/16-1, Si 438/24 and Si 438/28 that fund S.S., and K.W for research projects in central Argentina. MG Lopez de Luchi thanks fruitful discussion on Sierras Pampeanas geology with Dr. Rapalini, Dr. C. Martínez Dopico and Dr. E. Rossello. Gabriel Giordanengo and E. Llambías from the INGEIS are thanked for their technical support. Editorial handling by. Dr. N. Eby is specially acknowledged. Thoughtful reviews by Dra. Flavia Salani and Dra. Luana Moreira Florisbal are greatly appreciated since they contributed to the improvement of the present contribution.

Appendix 1. Main lithological features

The porphyritic rocks of the Granite Suite are composed of 3 to 8 cm K-feldspar (microcline) megacrysts, which are poikilitic with large inclusions of plagioclase and are mantled by zones that contain oriented inclusions of plagioclase (An_{35} to An_{25}), biotite, and variable amounts of amphibole (if hornblende is present among the mafic minerals) aligned along the visible euhedral zoning. Locally subhedral quartz inclusions are observed in the border of the bigger megacrysts. The coarse-grained groundmass is made up of plagioclase crystals which display oscillatory zoning in an overall normal trend. Observed An contents range from 10% to 45% with the more calcic and corroded cores in the amphibole-bearing porphyritic granitoids. Plagioclase crystals enclosed by K-feldspar phenocrysts are usually overgrown by a thin rim of albite, probably of subsolidus origin. Abundant sphene of up to 5mm is a common accessory mineral together with apatite, zircon, allanite, and magnetite.

In the equigranular facies of the Granite Suite, muscovite is a primary magmatic phase in some highly evolved granites of the central part of the Renca Batholith, as well as in the outer rim of the southeastern sector of the Las Chacras-Potrerillos batholith where apatite and opaque minerals are common accessories. However, zircon, sphene, and allanite are rarer. Plagioclase has normal zoning from An_{35}–An_{20} and is more sodic in the RG of the LCHPB, An_{20}–An_5. K-feldspar is poikilitic anhedral microcline, and biotite is the dominant mafic phase. Accessory minerals include apatite, zircon, and very scarce allanite and magnetite.

Rocks of the Monzonite suite are represented by stocks, mafic microgranular enclaves and synplutonic dikes. Mafic microgranular enclaves are widespread and abundant in the porphyritic facies of the Granite Suite and in the Monzonitic stocks. They appear either isolated or in enclave swarms and are porphyritic or equigranular. Isolated enclaves are texturally more uniform and probably represent different stages of mingling and mixing of the Monzonitic Suite magmas and high-K magmas of the Granite Suite (López de Luchi, 1996). Synplutonic dikes that intrude both the porphyritic facies of the Granite Suite and the monzonite stocks of the Renca Batholith and enclave swarms indicate that the monzonitic magma intruded into an almost solidified host, which resulted in the formation of a mingled hybrid matrix in the swarms. Locally fine-grained margins of the dikes suggest chilling against the colder crystallizing host. In many cases, syn-plutonic dikes grade into enclave swarms along the strike that is parallel to the foliation of the porphyritic host. Shapes of the individual enclaves are generally ovoid, although the larger ones, which could be up to 1m in length are more variable and tend to be tabular (López de Luchi, 1996). Xenocryst from the granite (e.g. plagioclase, quartz, porphyritic K-feldspar) were included in the marginal zones of the monzonite dikes

Textures and modes differ depending on the size of the enclaves. These rocks are monzonite, monzodiorite and minor monzogabbro and quartz monzonite. The distinctive magnesian and potassic character of most of these rocks led us to use specific nomenclature i.e. vaugnerites which are Mg–K meladiorites/monzonite and durbachites which are even more magnesian and potassic equivalents (Ferré and Leake, 2001; López-Moro and López-Plaza, 2004; Sabatier, 1991, and references therein). The MME and synplutonic dikes share some common textural features, irrespective of their bulk composition: long, needle-like apatite crystals which occurs particularly either in the outer rims of the plagioclase or in the groundmass, euhedral titanite and subhedral to anhedral crystals of mafic minerals either isolated or in clots. Subhedral plagioclase in all the Monzonite Suite rocks can be divided petrographically into two main types: crystals with zonal rims surrounding skeletal or honeycomb cores and completely zoned crystals. In both cases, oscillatory zoning is well developed in a mainly overall normal trend.

Based on the petrographic features, modes and chemistry (see below) MME were separated in five types (Table 2). Types 1 and 4 are porphyritic whereas Types 2, 3 and 5 are equigranular.

Porphyritic MME and stocks are amphibole biotite monzonite, monzodiorite, i.e. vaugnerite and durbachite. The most common (Types 1, 3, and 4) dm-to-m enclaves are monzonite, and silica-poor monzonite/monzodiorite (Table 1) and display in the groundmass either fine-grained doleritic textures or an interlocking anhedral of poikilitic K-feldspar and/or quartz. Porphyritc rocks of the Monzonite Suite are characterized by the development of K-feldspar megacryst, which, in some, mostly match the size of those in the host porphyritic granitoid. Some megacrysts cut across the contact between the enclave and granite host, whereas others are completely included, especially in the porphyritic monzonite stocks or along the border of the synplutonic dikes. Quartz ocelli and felsic segregation surrounded by amphibole–biotite are less frequent, but well-developed. Both types of felsic ocellar structures as well as the K megacryst are related to thermal and compositional interactions of (hydrous) mafic magma batches with co-existing granitic magmas (López de Luchi, 1996).

The porphyritic rocks (Types 1 and 4) contain subhedral elongated laths of plagioclase that show an overall trend of continuous normal zoning (An_{60} to An_{26}) with intermediate oscillatory rims in which the limits of the different compositional zones are well defined. Hornblende

is mostly present in all samples and shows subhedral-to-anhedral shapes, in many cases with cores of partially replaced clinopyroxene. Amphibole crystals poikilitically enclose small euhedral crystals of plagioclase, biotite, sphene, and rare clinopyroxene. Additional accessory phases are magnetite and rarer allanite. Textural relationships between the ferromagnesian minerals suggest partial replacement of clinopyroxene by hornblende – generally in the internal part of the enclaves – and of hornblende by biotite, primarily in the outer portions of enclaves.

The more mafic and smaller enclaves that range from monzogabbro to SiO_2 poor monzonite (Type 5) which appears only in the monzonitic stocks of the RB and San José del Morro pluton, are also vaugneritic but with very high MgO content. They contain rare plagioclase megacrysts that usually display reverse zoning with a corroded, more Ab-rich core (An_{40} to An_{25}) and more calcic plagioclase rims. K-feldspar is ameboidal-to-interstitial or appears as groups of radiating aggregates.

Only at two localities in the porphyritic facies of the Renca Batholith equigranular biotite monzonite (Type 2) enclaves compositionally equivalent to appinites (Fowler and Henney, 1996 and references therein) were found (Table 2) They are generally smaller (5–20 cm in diameter) than the rest of the Monzonite Suite enclaves. Accessory phases include zircon, allanite, apatite, magnetite, and ilmenite.

The monzonite stocks vary from medium- to fine-grained equigranular textures to very coarse-grained porphyritic textures with K-feldspar megacrysts, as in the case of GPG of the Las Chacras-Potrerillos Batholith. In other cases, plagioclase and amphibole phenocrysts in a fine-grained groundmass can be found. Although there are more variations in grain size, the overall pattern of the texture is similar to that of the enclaves and syn-plutonic dikes. Contacts with the host high-K granite suite are clearly delineated but in some cases like in the eastern limit of the monzonite stocks of the RB in part they are transitional.

Stocks are made up of plagioclase, amphibole (magnesiohornblende), K-feldspar, and sometimes quartz as major phases, as well as clinopyroxene apatite, titanite, allanite, and magnetite as accessory minerals. The plagioclase (20–40% modal) varies from a relatively homogeneous zonal andesine with rare oligoclase rims and fracture infillings, to, in other cases, a zoned plagioclase which ranges of An_{38}–An_{20} and exhibit honeycomb cores and rims with oscillatory zoning. Plagioclase crystals enclosed by K-feldspar phenocrysts are usually overgrown by a thin rim of exsolved albite. Mafic minerals are hornblende and biotite, either as clots with magnetite or as isolated crystal. Disaggregation of the less mixed monzonite rocks most likely led to the development of mafic clots in which amphibole with clinopyroxene cores, sphene, and magnetite are surrounded by biotite. The amphibole content (5–25% modal) increases with the rock color index. Biotite crystals (15–30% modal) range from subhedral to anhedral and, in many cases, include apatite and rarer allanite. Zoned and twinned epidote around allanite or as isolated crystal is occasionally found. In some cases, this includes tiny subhedral sphene crystals. In GPG, accessory apatite and sphene reach up to 1 cm, and the mantling of the K-feldspar by plagioclase is well developed.

Appendix 2. Analytical procedure

A total of 146 major- and trace element analyses are considered in this study, 53 of which are new analyses for the Monzonite suite rocks (Table 3). Published data for the Las Chacras-Potrerillos batholith were taken from López de Luchi et al. (2001, 2007) and from Lira and Ripley (1992), for the Renca batholith from López de Luchi (1996) and López de Luchi et al. (2007), for La Totora Batholith from López de Luchi et al. (2007), for the San José del Morro pluton from Quenardelle (1995). New determinations were performed on samples up to 10 k that were screened for alteration in hand specimens and thin sections. Samples were broken using an iron hammer and further reduced using an iron-plated jaw crusher and, subsequently, agate mills. Data for all the samples of the Renca Batholith were performed at Act Lab with Research resolution Method comprised ICP/MS for trace elements and X-ray fluorescence spectrometry (XRF) for major elements. Data for all the samples of the Las Chacras-Potrerillos and La Totora batholiths and the two samples of El Hornito pluton were done at the GeoForschungs Zentrum, Potsdam. Major element oxides and the trace elements Ba, Cr, Nb, Ni, Rb, Sr, V, Y, Zn, and Zr were analyzed using XRF and 105 °C dried samples were prepared as fused disks of Spectromelt® A12 (sample-to-flux ratio 1:6). A Siemens SRS 303 AS computerized spectrometer and matrix correction programs were used to calculate concentrations. H_2O^+ and CO_2 were measured IR-spectroscopically, following thermal decomposition at 1100 °C under oxygen atmosphere using LECO RC-412. The determination of rare earth elements was done with ICP-AES, following sample dissolution using the Na_2O_2-sinter technique and then separation and concentration using ion-exchange chromatography (Zuleger and Erzinger, 1988).Twenty new Nd and Sm isotopic analyses were performed on representative samples by conventional isotope dilution technique. The samples were weighed into Teflon vials and spiked with a suitable amount of ^{150}Nd–^{149}Sm spike solution prior to dissolution in a mixture of 2 ml HF and1 ml HNO3 with a PicoTrace™ digestion system. The solutions were processed by standard cation-exchange techniques for purification of the Sm and Nd fractions. For the determination of isotopic compositions, Sm and Nd were loaded with 2.5 N HCl on preconditioned double Re filaments. Measurements of isotopic ratios were performed on a thermal ionization mass spectrometer (TIMS) Finnigan Triton measuring in static mode (GZG, Dept. Isotope Geology). Repeated measurement of the Nd inhouse standard yielded a $^{143}Nd/^{144}Nd$ ratio of 0.511798 ± 0.000077 ($n = 71, 2\sigma$) over the course of this study. The obtained Nd isotopic ratios of the samples were normalized to a $^{146}Nd/^{144}Nd$ ratio of 0.7219. Total procedure blanks were consistently below 150 pg for Sm and Nd. All $1^{43}Nd/^{144}Nd$ ratios are reported with their 2σ internal precision plus the uncertainties resulting from the spike correction. Eight strontium, neodymium, and samarium whole-rock concentrations and isotopic compositions were taken from published data (see table for references). Chemical data were processed with GCD kit (Janoušek, 2000a, 2000b) and Petrograph v2 beta (Petrelli et al., 2005). Initial ratios for Sr isotopes and isochrons were recalculated with IsoPlot v.3.

References

Aceñolaza, F.G., Miller, H., Toselli, A.J., 1988. The Puncoviscana Formation (late Precambrian–early Cambrian). Sedimentology, tectonometamorphic history and age of the oldest rocks of NW Argentina. In: Bahlburg, H., Breitkreuz, C., Giese, P. (Eds.), The Southern Central Andes: Contribution to Structure and Evolution of an Active Continental Margin. Lecture Notes on Earth Sciences 17, pp. 25–38.

Aceñolaza, F.G., Miller, H., Toselli, A.J. (Eds.), 1990. El Ciclo Pampeano en el Noroeste Argentino. Serie Correlación Geológica 4, pp. 1–227.

Altherr, R., Holl, A., Hegner, E., Langer, C., Kreuzer, H., 2000. High-potassium, calc–alkaline I-type plutonism in the European Variscides: northern Vosges (France) and northern Schwarzwald (Germany). Lithos 50 (1–3), 51–73.

Anderson, J.L., 1996. Status of thermobarometry in granitic batholiths. Transactions of the Royal Society of Edinburgh 87, 125–138.

Barbarin, B., Didier, J., 1992. Genesis and evolution of mafic microgranular enclaves through various types of interaction between coexisting felsic and mafic magmas. Transactions of the Royal Society of Edinburgh: Earth Sciences 83, 145–153.

Bonin, B., 2004. Do coeval mafic and felsic magmas in post-collisional to within-plate regimes necessarily imply two contrasting, mantle and crustal, sources? A review. Lithos 78, 1–24.

Booker, J.R., Favetto, A., Pomposiello, M.C., 2004. Low electrical resistivity associated with plunging of the Nazca flat slab beneath Argentina. Nature 429, 399–403.

Brogioni, N., 1991. Caracterización petrográfica y geoquímica del Batolito de Las Chacras-Piedras Coloradas, San Luis, Argentina. 6 º Congreso Geológico Chileno, Actas. 1. Viña del Mar., pp. 766–770.

Brogioni, N., 1993. El Batolito Las Chacras-Piedras Coloradas, Prov. de San Luis. Geocronología y ambiente tectónico. Actas 12° Congreso Geológico Argentino y 2° Congreso de Exploración de Hidrocarburos. 4, pp. 54–60 Asociación Geológica Argentina, Mendoza, Argentina.

Bussy, F., Hernandez, J., von Raumer, J., 2000. Bimodal magmatism as a consequence of the post-collisional readjustment of the thickened Variscan continental lithosphere (Aiguilles Rouges-Mount Blanc Massif, Western Alps). Transactions of the Royal Society of Edinburgh, Earth Science 91, 221–233.

Cawood, P., 2005. Terra Australis Orogen: Rodinia breakup and development of the Pacific and Iapetus margins of Gondwana during the Neoproterozoic and Palaeozoic. Earth Science Reviews 69, 249–279.
Clemens, J.D., Bezuidenhout, A., 2014. Origins of coexisting diverse magmas in a felsic pluton: the Lysterfield granodiorite, Australia. Contributions to Mineralogy and Petrology 167, 991–1014.
Clemens, J.D., Mawer, C.K., 1992. Granitic magma transport by fracture propagation. Tectonophysics 204, 339–360.
Clemens, J.D., Regmi, K., Nicholls, I.A., Weinberg, R., Maas, R., 2016. The Tyonong pluton, its mafic synplutonic sheets and microgranular enclaves: the nature of the mantle connection in I-tye granitic magmas. Contributions to Mineralogy and Petrology 171 (35-).
Collins, W.J., Richards, S.R., Healy, B.E., Ellison, P.I., 2000. Origin of heterogeneous mafic enclaves by two-stage hybridisation in magma conduits(dykes) below and in granitic magmatic chambers. Transactions of the Royal Society of Edinburgh: Earth Sciences 91, 27–45.
Currie, C.A., Beaumont, C., Huismans, R.S., 2007. The fate of subducted sediments: a case for backarc intrusion and underplating. Geology 35, 1111–1114.
Dahlquist, A., Alasino, P.H., Eby, G.N., Galindo, C., Casquet, C., 2010. Fault controlled Carboniferous A-type magmatism in the Proto-Andean foreland (Sierras Pampeanas, Argentina): geochemical constraints and petrogenesis. Lithos 115, 65–81.
Davies, J.H., von Blackenburg, F., 1995. Slab breakoff: a model of lithosphere detachment and its test in the magmatism and deformation of collisional orogens. Earth and Planetary Science Letters 129, 852–872.
De Hollanda, M.H.B.M., Pimentel, M.M., Jardim de Sá, E.F., 2003. Paleoproterozoic subduction-related metasomatic signatures in the lithospheric mantle beneath NE Brazil: inferences from trace element and Sr–Nd–Pb isotopic compositions of Neoproterozoic high-K igneous rocks. Journal of South American Earth Sciences 15 (8), 885–900.
Debon, F., Lemmet, M., 1999. Evolution of Mg/Fe ratios in Late Variscan plutonic rocks from the external crystalline massifs of the Alps (France, Italy). Journal of Petrology 40 (7), 1151–1185.
DePaolo, D.J., Linn, A.M., Schubert, G., 1991. The continental crustal age distribution. Methods of determining mantle separation ages from Sm-Nd isotopic data and application to the Southwestern United States. Journal of Geophysical Research 96 (B2), 2071–2088.
Didier, J., Barbarin, B., 1991. Enclaves and granite petrology. Developments in Petrology. 13. Elsevier, Amsterdam.
Drobe, M., López de Luchi, M.G., Steenken, A., Siegesmund, S., Wemmer, K., 2009. Provenance of the late Proterozoic to early Cambrian meta-clastic sediments of the Sierra de San Luis (Eastern Sierras Pampeanas) and the southern Puna (Argentina). Journal of South America Earth Sciences 28, 239–262.
Drobe, M., López de Luchi, M.G., Steenken, A., Wemmer, K., Naumann, R., Frei, R., Siegesmund, S., 2011. Geodynamic Evolution of the Eastern Sierras Pampeanas based on geochemical, Sm-Nd, Pb-Pb and SHRIMP data. In: Siegesmund, S., Basei, M., Oyhantcabal, P. (Eds.), Multiaccretional Tectonics at the Rio de La Plata Margins. International Journal Earth Sciences 100(2), pp. 631–657.
Eby, G.N., 1992. Chemical subdivision of the A-type granitoids: petrogenetic and tectonic implications. Geology 20, 641–644.
Elburg, M.A., 1996. U-Pb ages and morphologies of zircon in microgranitoid enclaves and peraluminous host granite: evidence for magma mingling. Contributions to Mineralogy and Petrology 123 (2), 177–189.
Ferré, E.C., Caby, R., Peucat, J.J., Capdevila, R., Monié, P., 1998. Pan-African post-collisional ferro-potassic granite and quartz-monzonite plutons of Eastern Nigeria. Lithos 45, 255–278.
Ferré, E.C., Leake, B.E., 2001. Geodynamic significance of early orogenic high-K crustal and mantle melts: example of the Corsica Batholith. Lithos 59 (1), 47–67.
Florisbal, L.M., Bitencourt, M.F., Nardi, L.V.S., Conceicao, R.V., 2009. Early post-collisional granitic and coeval mafic magmatism of medium- to high-K tholeiitic affinity within the Neoproterozoic Southern Brazilian Shear Belt. Precambrian Research 175, 135–148.
Fowler, M.B., Henney, P.J., 1996. Mixed Caledonian appinite magmas: implications for lamprophyre fractionation and high Ba-Sr granite genesis. Contributions to Mineralogy and Petrology 126, 199–215.
Frost, B.R., Barnes, C.G., Collins, W.J., Arculus, R.J., Ellis, D.J., Frost, C.D., 2001. A geochemical classification of the igneous rocks. Journal of Petrology 42 (11), 2033–2048.
Fu, L., We, J., Kusky, T.M., Chen, H., Tan, J., Li, Y., Kong, L., Jiang, Y., 2012. Triassic shoshonitic dykes from the northern North China craton: petrogenesis and geodynamic significance. Geological Magazine 149 (01), 39–55.
Gamble, J., Woodhead, J., Wright, I., Smith, I., 1996. Basalt and sediment geochemistry and magma petrogenesis in a transect from ocean island arc to rifted continental margin arc: the Kermadec–Hikurangi margin, SW Pacific. Journal of Petrology 37, 1523–1546.
Goldstein, S.L., Onions, R.K., Hamilton, P.J., 1984. A Sm–Nd isotopic study of atmospheric dusts and particulates from major river systems. Earth and Planetary Science Letters 70 (2), 221–236.
Grosse, P., Söllner, F., Báez, M.A., Toselli, A.J., Rossi, J.N., de la Rosa, D., 2008. Lower Carboniferous post-orogenic granites in central-eastern Sierra de Velasco, Sierras Pampeanas, Argentina: U–Pb monazite geochronology, geochemistry and Sr–Nd isotopes. International Journal of Earth Sciences 98 (5), 1001–1025.
Harris, N.B.W., Pearce, J.A., Tindle, A.G., 1986. Geochemical characteristics of collision-zone magmatism. In: Coward, M.P., Ries, A.C. (Eds.), Collision Tectonics. Geological Society Special Publications 19, pp. 67–81 (London).
Harrison, T.M., Watson, E.B., 1984. The behavior of apatite during crustal anatexis: equilibrium and kinetic considerations. Geochimica et Cosmochimica Acta 48, 1467–1477.
Hildebrand, R.S., Whalen, J.B., 2014. Arc and slab failure magmatism in Cordilleran batholiths II: the Cretaceous Peninsular Ranges batholith of Southern and Baja California. Geoscience Canada 41, 399–458.
Holden, P., Halliday, A.N., Stephens, W.E., Henney, P.J., 1991. Chemical and isotopic evidence for major mass transfer between mafic enclaves and felsic magma. Chemical Geology 92, 135–152.
Hunen, J., Allen, M., 2011. Continental collision and slab break off: a comparison of 3D numerical models with observations. Earth and Planetary Science Letters 302, 27–37.
Huppert, H.E., Sparks, R.S.J., 1988. The generation of granitic magmas by intrusions of basalts into continental crust. Journal of Petrology 29 (3), 599–624.
Iannizzotto, N.F., López de Luchi, M.G., 2012. Geotermobarometría en suites monzoníticas y graníticas de los batolitos devónicos de las Sierras de San Luis. Serie Correlación Geológica 28 (2), 39–52 (Tucumán).
Janoušek, V., 2000a. Interpretation of the whole-rock geochemical data using the R language – the current state of affairs. In: Uher, P., Broska, I., Jeleň, S., Janák, M. (Eds.), Mineralogicko-petrologické sympózium Magurka '2000. 16.
Janoušek, V., 2000b. R - an alternative to spreadsheets and special software for geochemical calculations and plotting. Geolines 10, 34–35.
Janoušek, V., Bowes, D.R., Rogers, G., Farrow, C.M., Jelinek, E., 2000. Modelling diverse processes in the petrogenesis of a composite batholith; the Central Bohemian Pluton, Central European Hercynides. Journal of Petrology 41, 511–543.
Janoušek, V., Braithwaite, C.J.R., Bowes, D.R., Gerdes, A., 2004. Magma-mixing in the genesis of Hercynian calc–alkaline granitoids: an integrated petrographic and geochemical study of the Sázava intrusion, Central Bohemian Pluton, Czech Republic. Lithos 78, 67–99.
Jiang, Y.H., Jiang, S.Y., Ling, H.F., Zhou, X.R., Rui, X.Y., Yang, W.Z., 2002. Petrology and geochemistry of shoshonitic plutons from the western Kulum orogenic belt, northwest Xinyiang, China: implications for granitoid genesis. Lithos 63, 165–187.
Jiang, Y.H., Liu, Z., Jia, R.-Y., Liao, S.-Y., Zhou, Q., Zhao, P., 2012. Miocene potassic granite–syenite association in western Tibetan Plateau: implications for shoshonitic and high Ba–Sr granite genesis. Lithos 134-135, 146–162.
Jung, S., Pfander, J., 2007. Source composition and melting temperatures of orogenic granitoids:constraints from CaO/Na_2O, Al_2O_3/TiO_2 and accessory mineral saturation thermometers. European Journal of Mineralogy 19, 859–870.
Kay, S., Orrell, S., Abbruzzi, J.M., 1996. Zircon and whole rock Nd–Pb isotopic evidence for a Grenville Age and a Laurentian origin for the basement of the Precordillera in Argentina. The Journal of Geology 104, 637–648.
Kemp, A.I.S., 2003. Plutonic boninite-like rocks in an anatectic setting: tectonic implications for the Delamerian orogen in southeastern Australia. Geology 31 (4), 371–374.
Lira, R., Ripley, E.M., 1992. Hydrothermal alteration and REE-Th mineralization at the Rodeo de Los Molles deposit, Las Chacras batholith, central Argentina. Contributions to Mineralogy and Petrology 110, 370–386.
Llambías, E.J., Sato, A.M., Ortiz Suárez, A., Prozzi, C., 1998. The granitoids of the Sierra de San Luis. In: Pankhurst, R.J., Rapela, C.W. (Eds.), The Proto-Andean Margin of Gondwana. Geological Society of London Special Publication 142, pp. 325–341.
López de Luchi, M.G, 1986. Geología y Petrología del basamento de la Sierra de San Luis, Región del Batolito de Renca. PhD Thesis, Departamento de Geología. Facultad de Ciencias Exactas. Universidad de Buenos Aires, p. 374.
López de Luchi, M.G., 1987. Caracterización geológica y geoquímica del Plutón La Tapera y del Batolito de Renca, Sierra de San Luis. 10º Congreso Geológico Argentino, Tucumán. Actas 4, 84–87.
López de Luchi, M.G., 1996. Enclaves en un Batolito Postectónico: Petrología de los enclaves microgranulares del Batolito de Renca. Revista de la Asociación Geológica Argentina 51 (2), 131–146.
Lopez de Luchi, M.G., Siegesmund, S., Hofmann, A., Hübner, H., Hulka, C., Mosch, S., 2001. Geological setting and composition of the Las Chacras-Potrerillos Batholith, Sierras Pampeanas, Argentina: first results. Zeitschrift der Deutschen Geologischen Gesellschaft 152 (2-3), 325–350.
López de Luchi, M.G., Rapalini, A.E., Rossello, E., Geuna, S., 2002. Rock and magnetic fabric of the Renca Batholith (Sierra de San Luis, Argentina): constraints on its emplacement. Lithos 61, 161–186.
López de Luchi, M.G., Rapalini, A.E., Siegesmund, S., Steenken, A., 2004. Application of magnetic fabrics to the emplacement and tectonic history of Devonian granitoids in Central Argentina. In: Martín-Hernández, F., Luneburg, C., Aubourg, C., Jackson, M. (Eds.), Magnetic Fabric: Methods and Applications. Geological Society of London Special Publication 238, pp. 447–474.
López de Luchi, M.G., Favetto, A., Pomposiello, M.C., Booker, J., 2005. Magnetotelluric evidence for the suture between the Río de la Plata and the Pampean cratons at 31°40′, Córdoba province, Argentina. Extended Abstracts 6th International Symposium on Andean Geodynamics, (ISAG 2005, Barcelona), pp. 446–449 (ISBN 2-7099-1575-8).
López de Luchi, M.G., Siegesmund, S., Wemmer, K., Steenken, A., Naumann, R., 2007. Geochemical constraints on the petrogenesis of the Paleozoic granitoids of the Sierra de San Luis, Sierras Pampeanas, Argentina. Journal of South America Earth Sciences 24, 138–166.
López de Luchi, M.G., Steenken, A., Martínez Dopico, C.I., Drobe, M., Wemmer, K., Siegesmund, S., 2010. Sm–Nd isotopic constraints on the Neoproterozoic –early Paleozoic evolution of the Eastern Sierras Pampeanas. Bolletino di Geofisica teorica ed applicata 51, 31–33.
López-Moro, F.J., López-Plaza, M., 2004. Monzonitic series from the Variscan Tormes Dome (Central Iberian Zone): petrogenetic evolution from monzogabbro to granite magmas. Lithos 72, 19–44.
Luo, B.-J., Zhang, H.-F., Xu, W.-C., Guo, L., Pan, F.-B., Yang, H., 2015. The Middle Triassic Meiwu Batholith, West Qinling, Central China: implications for the evolution of compositional diversity in a composite batholith. Journal of Petrology 56 (6), 1139–1172.
Middlemost, E.A.K., 1994. Naming materials in the magma/igneous rock system. Earth Science Reviews 37, 215–224.

Middlemost, E.A.K., 1997. Magmas, Rocks and Planetary Development. Longman, Harlow (299 pp.).
Moyen, J.-F., Stevens, G., 2006. Experimental constraints on TTG petrogenesis: implications for Archean geodynamics. In: Benn, K., Mareschal, J.-C., Condie, K.C. (Eds.), Archean Geodynamics and Environments. monographs. AGU, pp. 149–178.
Ortiz, Suárez A., Grosso, Cepparo P., Gómez, Figueroa J., Erroz, M., Montenegro, T., 2009. Geología del basamento en el extremo noroeste de la sierra de San Luis. Revista de la Asociación Geológica Argentina 64, 481–492.
Osterhus, L., Jung, S., Berndt, J., Hauff, F., 2014. Geochronology, geochemistry and Nd, Sr and Pb isotopes of syn-orogenic granodiorites and granites (Damara orogen, Namibia): arc-related plutonism or melting of mafic crustal sources? Lithos 200–201, 386–401.
Pankhurst, R.J., Rapela, C.W., Saavedra, J., Baldo, E., Dahlquist, J., Pascua, I., Fanning, C.M., 1998. The Famatinian magmatic arc in the central Sierras Pampeanas: an Early to Mid-Ordovician continental arc on the Gondwana. In: Pankhurst, R.J., Rapela, C.W. (Eds.), The Proto-Andean Margin of Gondwana. Geological Society of London Special Publication 142, pp. 343–367.
Pankhurst, R.J., Rapela, C.W., Fanning, C.M., 2000. Age and origin of coeval TTG, I and S-type granites in the Famatinian belt of NW Argentina. Transactions of the Royal Society of Edinburgh, Earth Science 91, 151–168.
Peacock, M.A., 1931. Classification of igneous rocks suites. Journal of Geology 39, 54–67.
Pearce, J.A., 1996. Sources and settings of granitic rocks. Episodes 19 (4), 120–125.
Pearce, J.A., Harris, N.B., Tindle, A.G., 1984. Trace-element discrimination diagrams for the tectonic interpretation of granitic rocks. Journal of Petrology 25, 956–983.
Pearce, J.A., Stern, R.J., Bloomer, S.H., Fryer, P., 2005. Geochemical mapping of the Mariana arc-basin system: implications for the nature and distribution of subduction components. Geochemistry, Geophysics, Geosystems 2005 (6), Q07006. http://dx.doi.org/10.1029/2004GC000895.
Petford, N., Gallagher, K., 2001. Partial melting of mafic (amphibolitic) lower crust by periodic influx of basaltic magma. Earth and Planetary Science Letters 193, 483–489.
Petford, N., Kerr, R.C., Lister, J.R., 1993. Dike transport of granitoid magmas. Geology 21, 845–848.
Petrelli, M., Poli, G., Perugini, D., Peccerillo, A., 2005. PetroGraph: a new software to visualize, model, and present geochemical data in igneous petrology. Geochemistry, Geophysics, Geosystems 6, Q07011. http://dx.doi.org/10.1029/2005GC000932.
Pin, C., Binon, M., Belin, J.M., Barbarin, B., Clemens, J.D., 1990. Origin of microgranular enclaves in granitoids: equivocal Sr-Nd evidence from Hercynian rocks of Massif Central, France. Journal of Geophysical Research 95, 17821–17828.
Pinotti, L.P., Coniglio, J.E., Esparza, A.M., D'Eramo, F.J., Llambias, E.J., 2002. Nearly circular plutons emplaced at shallow crustal levels, Cerro Aspero batholith, Sierras Pampeanas de Córdoba, Argentina. Journal of South America Earth Sciences 15, 251–265.
Prozzi, C., Ramos, G., 1988. La Formación San Luis. Primeras Jornadas de Trabajo de Sierras Pampeanas San Luis, Argentina, Abs. 1.
Quenardelle, S., 1995. Petrografía y geoquímica del plutón San José del Morro, provincia de San Luis. Revista de la Asociación Geológica Argentina 50 (1-4), 229–236.
Ramos, V.A., 2008. The basement of the Central Andes: the Arequipa and related terranes. Annual Review of Earth and Planetary Sciences 36, 289–324.
Ramos, V.A., Jordan, T.E., Allmendinger, W., Mpodozis, C., Kay, S.M., Cortés, J.M., Palma, M., 1986. Paleozoic terranes of the Central Argentine–Chilean Andes. Tectonics 5, 855–880.
Ramos, V.A., Cristallini, E.O., Pérez, D.J., 2002. The Pampean flat-slab of the Central Andes. Journal of South American Earth Sciences 15, 59–78.
Rapela, C.W., Pankhurst, R.J., Casquet, C., Baldo, E., Saavedra, J., Galindo, C., Fanning, C.M., 1998. The Pampean Orogeny of the southern proto-Andes: Cambrian continental collision in the Sierras de Córdoba. In: Pankhurst, R.J., Rapela, C.W. (Eds.), The Proto-Andean Margin of Gondwana. Geological Society of London Special Publication 142, pp. 181–217.
Rapela, C.W., Pankhurst, R.J., Casquet, C., Baldo, E., Galindo, C., Fanning, C.M., Saavedra, J., 2001. Ordovician metamorphism in the Sierras Pampeanas: new U–Pb SHRIMP ages in central-east Valle Fértil and the Velasco Batholith. Extended Abstract Volume 3rd South American Symposium on Isotope Geology, pp. 616–619.
Rapela, C.W., Pankhurst, R.J., Casquet, C., Fanning, C.M., Baldo, E.G., Gonzáles-Casado, J.M., Galindo, C., Dahlquist, J., 2007. The Río de la Plata craton and the assembly of Gondwana. Earth-Science Reviews 83, 49–82.
Rapela, C.W., Baldo, E.G., Pankhurst, R.J., Fanning, C.M., 2008. The Devonian Achala Batholith of the Sierras Pampeanas: F-rich aluminous A-type granites. Abstracts 6th South American Symposium on Isotope Geology. 1, p. 104.
Rapp, R.P., Watson, E.B., 1995. Dehydration melting of metabasalt at 8–32 kbar: implications for continental growth and crust–mantle recycling. Journal of Petrology 36, 891–931.
Rickwood, P.C., 1989. Boundary lines within petrologic diagrams which use oxides of major and minor elements. Lithos 22 (4), 247–263.
Sabatier, H., 1991. Vaugnerites: special lamprophyre-derived mafic enclaves in some Hercynian granites from Western and Central Europe. In: Didier, J., Barbarin, B. (Eds.), Enclaves and Granite Petrology. Elsevier, Amsterdam, pp. 63–81.
Sato, A.M., González, P.D., Petronilho, L.A., Llambías, E.J., Varela, R., Basei, M.A., 2001. Sm–Nd, Rb–Sr and K–A age constraints of the El Molle and Barroso plutons, western Sierra de San Luis, Argentina. 3ª South America Symposium on Isotope Geology, Extended Abstract Volume (CD). Sociedad Geológica de Chile, Santiago, pp. 241–244.
Schaltegger, U., Brack, P., 2007. Crustal-scale magmatic systems during intracontinental strike-slip tectonics: U, Pb and Hf isotopic constraints from Permian magmatic rocks of the Southern Alps. International Journal of Earth Sciences 96 (6), 1131–1151.
Shand, S.J., 1943. The Eruptive Rocks. 2nd edition. John Wiley, New York (444 pp.).
Siegesmund, S., Steenken, A., López de Luchi, M.G., Wemmer, K., 2004. The Las Chacras-Potrerillos Batholith: structural evidence on its emplacement and timing of the intrusion. International Journal of Earth Sciences 93, 23–43.
Siegesmund, S., Steenken, A., Martino, R., Wemmer, K., López de Luchi, M.G., Frei, R., Presniakov, S., Guereschi, A., 2009. Time constraints on the tectonic evolution of the Eastern Sierras Pampeanas (Central Argentina). International Journal of Earth Sciences 99, 1199–1226.
Sims, J.P., Skirow, R.G., Stuart-Smith, P.G., Lyons, P., 1997. Informe geológico y metalogenético de las Sierras de San Luis y Comechingones (provincias de San Luis y Córdoba), 1:250000. Anales 28, IGRM, SEGEMAR, Buenos Aires, pp. 1–148.
Sims, J.P., Ireland, T.R., Camacho, A., Lyons, P., Pieters, P.E., Skirrow, R.G., Stuart-Smith, P.G., Miró, R., 1998. U–Pb, Th–Pb and Ar–Ar geochronology from the southern Sierras Pampeanas, Argentina: implications for the Paleozoic evolution of the western Gondwana margin. In: Pankhurst, J.R., Rapela, C.W. (Eds.), The Proto-Andean Margin of Gondwana. Geol Soc London Spec Public 142, pp. 259–281.
Steenken, A., López de Luchi, M.G., Siegesmund, S., Wemmer, K., 2002. An insight into the structural evolution of the Sierra de San Luis (southeastern Sierras Pampeanas, Argentina): a progress report. In: Cabaleri, N., Linares, E., de Luchi, López, Ostera, H., Panarello, H. (Eds.), Actas 15 Congreso Geológico Argentino. I, pp. 321–325.
Steenken, A., Wemmer, K., López de Luchi, M.G., Siegesmund, S., Pawlig, S., 2004. Crustal provenance and cooling of the basement complexes of the Sierra de San Luis: an insight into the tectonic history of the proto-Andean margin of Gondwana. Gondwana Research 7 (4), 1171–1195.
Steenken, A., Siegesmund, S., López de Luchi, M.G., Frei, R., Wemmer, K., 2006. Neoproterozoic to Early Palaeozoic Events in the Sierra de San Luis: Implications for the Famatinian Geodynamics in the Eastern.
Steenken, A., Wemmer, K., Siegesmund, S., López de Luchi, M.G., 2008. Time constraints on the Famatinian and Achalian structural evolution of the basement of the Sierra de San Luis (Eastern Sierras Pampeanas, Argentina). Journal of South America Earth Sciences 25, 336–358.
Steenken, A., López de Luchi, M.G., Martínez Dopico, C., Drobe, M., Wemmer, K., Siegesmund, S., 2011. The Neoproterozoic-Early Paleozoic metamorphic and magmatic evolution of the Eastern Sierras Pampeanas: an overview. In: Siegesmund, S., Basei, M., Oyhantcabal, P. (Eds.), Multiaccretional Tectonics at the Rio de La Plata Margins. International Journal of Earth Sciences 100(2), pp. 465–488.
Stuart-Smith, P.G., Camacho, A., Sims, J.P., Skirrow, R.G., Lyons, P., Pieters, P.E., Black, L.P., 1999. Uranium–lead dating of felsic magmatic cycles in the southern Sierras Pampeanas, Argentina: implications for the tectonic development of the proto-Andean Gondwana margin. In: Ramos, V.A., Keppie, J.D. (Eds.), Laurentia–Gondwana Connections before Pangea. Geological Society of America, Special Papers 336, pp. 87–114.
Sun, S.S., 1980. Lead isotope study of young volcanic rocks from mid-ocean ridges, ocean islands and island arcs. Philosophical Transactions of the Royal Society of London, Series A 297, 409–445.
Sun, S.S., McDonough, W.F., 1989. Chemical and isotopic systematics of oceanic basalts: implications for mantle composition and processes. In: Saunders, A.D., Norry, M.J. (Eds.), Magmatism in Ocean Basins. Geological Society Special Publications 42, pp. 313–345 (London).
Tatsumi, Y., Eggins, S., 1995. Subduction Zone Magmatism. Blackwell Science, Cambridge (211 pp.).
Taylor, S.R., McLennan, S.M., 1981. The composition and evolution of the continental crust: rare earth element evidence from sedimentary rocks. Philosophical Transactions Royal Society of London A 301, 381–399.
Topuz, G., Altherr, R., Siebel, W., Schwarz, W.H., Zack, T., Hasözbek, A., Barth, M., Satır, M., Şen, C., 2010. Carboniferous high-potassium I-type granitoid magmatism in the Eastern Pontides: the Gümüşhane pluton (NE Turkey). Lithos 116 (1-2), 92–116.
van de Flierdt, T., Hoernes, S., Jung, S., Masberg, P., Hoffer, E., Schaltegger, U., Friedrichsen, H., 2003. Lower crustal melting and the role of open-system processes in the genesis of syn-orogenic quartz diorite-granite-leucogranite associations: constraints from Sr–Nd–O isotopes from the Bandombaai Complex, Namibia. Lithos 67, 205–226.
Vernon, R.H., 1984. Micro-granitoid enclaves: globules of hybrid magma quenched in a plutonic environment. Nature 304, 438–439.
Watson, B.E., Harrison, M.T., 1983. Zircon saturation revisited: temperature and compositional effects in a variety of crustal magma types. Earth and Planetary Science Letters 64, 295–304.
Weaver, B.L., Tarney, J., 1984. Empirical approach to estimating the composition of the continental crust. Nature 310, 575–577.
Weinberg, R.F., Sial, A.N., Pessoa, R.R., 2001. Magma flow within the Tavares pluton, northeastern Brazil: compositional and thermal convection. Geological Society of America Bulletin 113, 508–520.
Whalen, J.B., Currie, K.L., Chappel, B.W., 1987. A type granites: geochemical characterization, discrimination and petrogenesis. Contributions to Mineralogy and Petrology 95, 407–419.
Whitney, J.A., 1988. The origin of granite: the role and source of water in the evolution of granitic magmas. Geological Society of America Bulletin 100, 1886–1897.
Willner, A.P., Gerdes, A., Massonne, H.-J., Schmidt, A., Sudo, M., Thomson, S.N., Vujovich, G., 2011. The geodynamics of collision of a microplate (Chilenia) in Devonian times deduced by the pressure–temperature–time evolution within part of a collisional belt (Guarguaraz Complex, W-Argentina). Contributions to Mineralogy and Petrology 162, 303–327.
Yao-Hui, J., Shao-Yong, J., Kui-Dong, Z., Hong-Fei, L., 2006. Petrogenesis of Late Jurassic Qianlishan granites and mafic dykes, Southeast China: implications for a back-arc extension setting. Geological Magazine 143, 457–474.
Zhang, C., Holtz, F., Koepke, J., Wolff, P.E., Ma, C., Bédard, J.H., 2013. Constraints from experimental melting of amphibolite on the depth of formation of garnet-rich restites, and implications for models of Early Archean crustal growth. Precambrian Research 231, 206–217.
Zuleger, E., Erzinger, J., 1988. Determination of the REE and Y in silicate materials with ICP-AES. Fresenius' Zeitschrift für Analytische Chemie 332, 140–143.